SPdKS ANALYSIS OF ULTRA-LOW VELOCITY ZONES BENEATH THE WESTERN PACIFIC

by

Kevin James Jensen

A thesis submitted to the faculty of
The University of Utah
in partial fulfillment of the requirements for the degree of

Master of Science

in

Geophysics

Department of Geology and Geophysics

The University of Utah

May 2013

The University of Utah Graduate School

STATEMENT OF THESIS APPROVAL

The following faculty members served as the supervisory committee chair and members for the thesis of Kevin James Jensen.

Dates at right indicate the members' approval of the thesis.

Michael S. Thorne, Chair	03/14/2013 Date Approved
Kristine L. Pankow, Member	03/14/2013 Date Approved
Keith D. Koper, Member	 Date Approved

The thesis has also been approved by Francis H. Brown, Dean of the College of Mines and Earth Sciences and by Donna M. White, Interim Dean of The Graduate School.

ABSTRACT

We collected a new data set of 1354 broadband *SPdKS* waveforms sampling the western Pacific Ocean region. These data indicate that multiple ultra-low velocity zones (ULVZs) exist in this region. We compared these data to synthetic seismograms computed with the axisymmetric finite difference method PSVaxi for a suite of 517 unique ULVZ models. The region beneath the North and South Philippine Sea shows no evidence for ULVZ presence. The region beneath the Coral Sea shows a large ULVZ, which is approximately 700 × 700 km in lateral dimensions and up to 20 km thick. Multiple small scale ULVZs approximately 180 × 180 km and up to 10 km thick are inferred beneath the South China Sea. Our findings are consistent with previous efforts utilizing the *ScP* seismic phase and provide additional constraints on ULVZ elastic parameters.

To my beloved wife, Kristina.

TABLE OF CONTENTS

ACKNOWLEDGEMENTS

I would like to thank Michael Thorne for the time and effort that he exerted in order to mentor and mold me into the scholar I am today. He always had high expectations of me and his love of science and his enthusiasm is contagious. I would also like to thank Sebastian Rost, Kris Pankow, and Keith Koper for their insights and suggestions.

Lastly, I would like to thank my wife, Kristina, for her patience with this whole process. She has been a source of encouragement and support in this effort.

CHAPTER 1

INTRODUCTION

Evidence for the existence of ultra-low velocity zones (ULVZs) has been put forth using a wide variety of seismic phases, including *SPdKS* [e.g., *Garnero et al.*, 1993; *Thorne and Garnero*, 2004], PcP [e.g., *Hutko et al.*, 2009; *Mori and Helmberger*, 1995], *ScP* [e.g., *Garnero and Vidale*, 1999; *Idehara*, 2011; *Rost and Revenaugh*, 2003], ScS [*Avants et al.*, 2006], PKP precursors [e.g., *Thomas et al.*, 1999; *Vidale and Hedlin*, 1998], and anomalies in travel-time or slowness of a variety of different phases [e.g., *Wen*, 2001; *Xu and Koper*, 2009]. ULVZ physical parameters have been reported with *S*-wave velocity reductions (δV_S) as large as 45% (all percentages reported with respect to the Preliminary Reference Earth Model [PREM; *Dziewonski and Anderson*, 1981], *P*-wave velocity reductions (δV_P) as large as 20%, density increases ($\delta\rho$) of up to 10%, and thicknesses (h) of up to 40 km [see *Thorne and Garnero*, 2004 for a review]. Nevertheless, strong tradeoffs exist in the model space resulting in uncertainty in many of these parameters [e.g., *Garnero and Helmberger*, 1998]. At most, 40% of the surface area of the core-mantle boundary (CMB) has been probed for ULVZs [see *McNamara et al.*, 2010 for a review of ULVZ coverage]. The greatest concentration of ULVZs found thus far are concentrated in the central and western Pacific region and may be associated with the edges of Large Low Shear Velocity Provinces (LLSVPs) [*Garnero and McNamara*, 2008; *McNamara et al.*, 2010]. However, the incomplete sampling of the CMB region makes this assertion difficult to assess. Constraining physical dimensions of ULVZs is difficult due to sparse CMB sampling.

Many hypotheses have been put forth to explain the origin of ULVZs. The most commonly cited origin is that ULVZs are partially molten [*Berryman*, 2000; *Williams and Garnero*,

1996]. In the case of a partial melt origin, a 3:1 V_S to V_P velocity reduction is expected. Many studies [e.g., *Revenaugh and Meyer*, 1997; *Rost et al.*, 2005] have demonstrated that waveforms are consistent with this 3:1 velocity reduction. A 3:1 velocity ratio is also consistent with iron enrichment of post-perovskite ensuing from core-mantle reactions [*Mao et al.*, 2006]. Nevertheless, a 3:1 velocity ratio has not been demonstrated as a necessity to predict ULVZ associated waveforms. A 1:1 or 2:1 velocity ratio may be more consistent with some waveforms, indicating a compositional component to ULVZ makeup [e.g., *Hutko et al.*, 2009; *Zhang et al.*, 2009]. A 2:1 velocity ratio is consistent with iron rich (Mg,Fe)O [*Wicks et al.*, 2010].

With the rise in availability of distributed memory computer systems recent efforts have begun modeling *SPdKS* waveforms with numerical techniques in 2+ dimensions. Rondenay *et al.* [2010] utilized a 2D pseudospectral technique and Thorne *et al.* [2013b] used the 2.5D axi-symmetric finite difference approach PSVaxi. Both studies demonstrated that *SPdKS* waveforms are highly sensitive to 2D ULVZ model geometries and are capable of mapping ULVZ position and lateral dimensions. In this paper, we examine the region beneath the western Pacific Ocean for evidence of ULVZs using the *SPdKS* seismic phase and the PSVaxi modeling approach to constrain ULVZ position and size. We compare these observations with ULVZs mapped in previous studies that used pre- and postcursors to the *ScP* seismic phase.

CHAPTER 2

SPdKS DATA

Decades of evidence have accumulated showing the existence of ULVZs in the western Pacific Ocean region. The majority of these studies have analyzed short period *ScP* data [*Garnero and Vidale*, 1999; *Idehara*, 2011; *Idehara et al.*, 2007; *Reasoner and Revenaugh*, 2000; *Rost and Revenaugh*, 2001; 2003; *Rost et al.*, 2006; *Rost et al.*, 2010; *Rost et al.*, 2005] or broadband *SPdKS* arrivals [*Garnero and Helmberger*, 1995; 1996; *Thorne and Garnero*, 2004; *Wen and Helmberger*, 1998]. *ScP* is an *S*-wave that converts to a *P*-wave upon reflection at the CMB (Figure 2.1a). The seismic phase *SPdKS* is related to the *ScP* phase as it is essentially an *ScP* wave that strikes the CMB at the angle for critical *P*-wave diffraction generating P_{diff} (*Pd*) segments that travel along the CMB. The *Pd* arcs can be generated along the CMB on either the source (*SPdKS*) or receiver-side (*SKPdS*) of the ray path (Figure 2.1a). For the PREM model [*Dziewonski and Anderson*, 1981], *SPdKS* first emerges at an epicentral distance of roughly 104° but is not well separated from *SKS* until roughly 110°. *SPdKS* waveforms are typically analyzed with respect to *SKS* (Figure 2.1a). *SKS* and *SPdKS* follow roughly the same path with the *Pd* arc along the CMB being the primary difference in ray path. It is assumed that any perturbation in the travel-time of *SPdKS* with respect to *SKS* is due to heterogeneity in the lowermost mantle along the CMB as this is where the two ray paths diverge. Between 110° and 115° *SPdKS* has been demonstrated to show the most distinctive waveform differences when compared to waveforms calculated for the PREM model [*Thorne and Garnero*, 2004], however ULVZ signature may be observed for records at distances as close as 105° [*Thorne et al.*, 2013b]. As the arrival distance increases past 115°, *SPdKS* waveforms behave more similarly to that predicted by the PREM

model. As the *Pd* path length increases (up to ~1500 km along the CMB for a 125° arrival) the effects of small scale ULVZ structure are less evident. We refer to the point where *Pd* initiates along the CMB as the *Pd*-inception point.

Multiple ULVZs have been detected with short period *ScP* arrivals in the western Pacific ocean region. Observations are summarized in Figure 2.1b (red/blue circles, crosses, diamonds indicate positive/negative sightings) with positive ULVZ sightings clustered into four main groups beneath the Philippines, Borneo, New Caledonia, and the Coral Sea. Broadband *SPdKS* arrivals have also been examined and are consistent with the existence of ULVZs in this region. Motivated by the presence of ULVZs in the western Pacific from multiple observations using *ScP* data, we collect broadband *SPdKS* data that may interact with these ULVZs. We collect data from the Incorporated Research Institutions for Seismology (IRIS) Data Management Center for events occurring along the Java, New Britain, Kermadec-Tonga, Ryukyu, and Marianas trenches from 1990 through 2010 with depths greater than 100 km, and with magnitudes: $5.8 \leq M_w \leq 7.5$. 466 events met these initial data quality requirements. We examined radial component data for stations from 90° to 100° epicentral distance to as sess the complexity of the source-time function [see, e.g., *Thorne and Garnero*, 2004]. Events that did not possess an impulsive source-time function were discarded. After this initial quality control step the dataset included 355 earthquakes.

Data were requested for these 355 events for stations between 100° to 125°. Radial component seismograms were band-pass filtered between 0.03 Hz to 1 Hz and visually inspected to ensure that the *SKS*, *SKKS*, and *Sdiff* (for appropriate distances) arrivals were clearly identifiable. If these arrivals could not be unquestionably identified the trace was discarded. Data were integrated to displacement and depth corrected to a common source depth of 500 km.

We focus on four regions with excellent data coverage within the western Pacific area. Figure 2.1b shows the *Pd* arcs along the CMB for *SPdKS* data collected in the focus regions. Throughout this paper, these regions are referred to as (1) the Coral Sea region, (2) the South Philippine Sea region, (3) the North Philippine Sea region, and (4) the South China Sea region (see Figure 2.1b). Data retained for these regions include a total of 40 events with 1354 *SPdKS*

seismograms in the distance range from 105° to 125° . *SPdKS* data collected for two regions (the Coral Sea and S. Philippine Sea regions) are shown in Figures 2.2a and 2.2c.

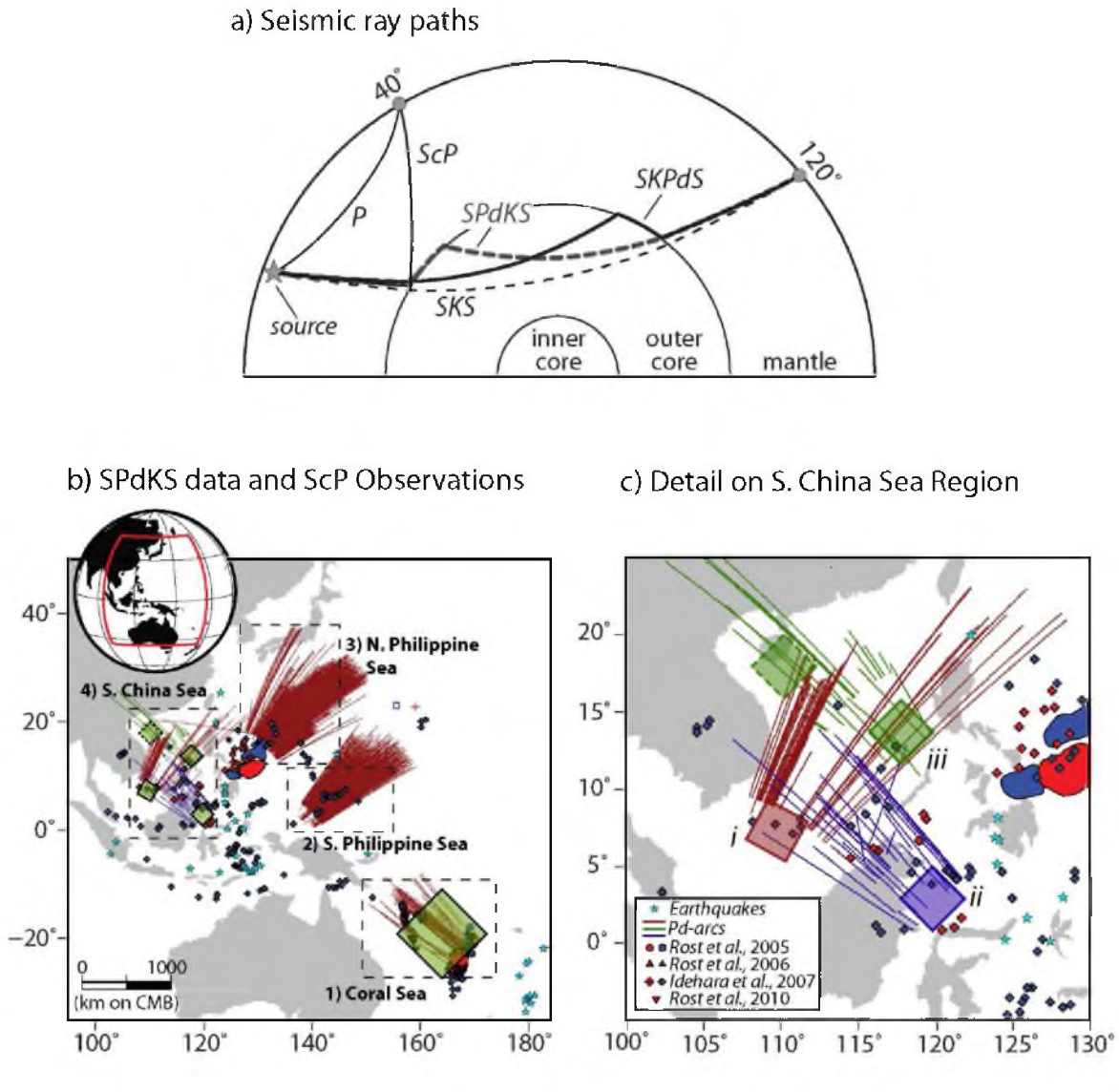

Figure 2.1 Raypath of SPdKS and the location of Pdiff on the CMB beneath the west Pacific. (a) *ScP* and *SPdKS* ray paths are shown where the *ScP* and direct *P*-arrivals (thin solid black lines) are drawn at an epicentral distance of 40°. The *SPdKS* (dashed gray line), *SKPdS* (heavy black line) and *SKS* (dashed black line) arrivals are drawn at 120°. (b) Data used in this study were divided into four geographic regions outlined by the dashed black boxes: (1) Coral Sea, (2) South Philippine Sea, (3) North Philippine Sea, and (4) South China Sea. Red lines show the Pd portion along the CMB of *SPdKS* data collected in this study. Red (blue) diamonds, circles, and triangles show *ScP* bouncepoints on the CMB that indicate ULVZ presence (non-presence) from the studies of [*Idehara et al.*, 2007; *Rost et al.*, 2006; *Rost et al.*, 2010; *Rost et al.*, 2005]. Similarly, regions outlined in red (blue) show areas inferred to contain ULVZs from the studies of [*Garnero and Vidale*, 1999; *Idehara*, 2011; *Reasoner and Revenaugh*, 2000; *Rost and Revenaugh*, 2001; 2003; *Rost et al.*, 2010]. ULVZs mapped in this study are drawn as green shaded boxes. (c) A zoomed in region on the S. China Sea is shown. *SPdKS* data for this region are subset into three groups: (*i*) red Pd-arcs, (*ii*) purple Pd-arcs, and (*iii*) green Pd-arcs. ULVZs inferred in this region are drawn with similarly shaded boxes.

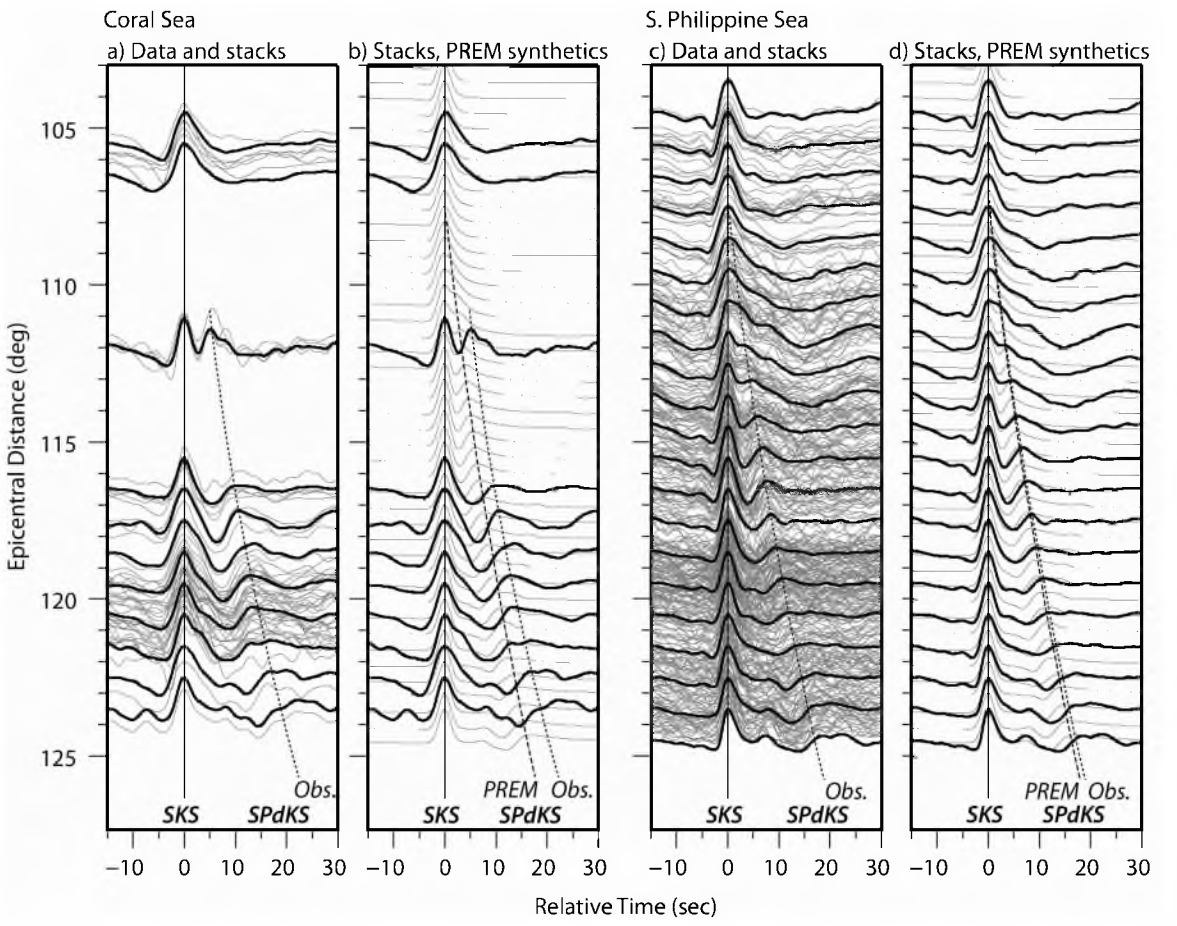

Figure 2.2. Data stack comparison to the PREM model for two regions. a) Data observations and comparison to PREM for the Coral Sea region. In the left profile the radial component seismograms (gray traces) are aligned on *SKS* showing the observed travel-time of *SPdKS* with stacks (black traces) overlaying them. The right profile shows PREM synthetics overlain by data stacks, both aligned on *SKS*. The PREM synthetic and observed arrivals of *SPdKS* are marked. b) Same as a) but for the S. Philippine Sea region.

CHAPTER 3

METHOD

In this paper we calculate synthetic seismograms using the PSVaxi approach [see, e.g., *Thorne et al.*, 2013a; *Thorne et al.*, 2013b]. PSVaxi computes *P/SV*- synthetic seismograms for 2D input models on a spherical grid with an expansion to 3D by rotation around the axis passing through the seismic source and the center of the Earth, generating models that are rotationally symmetric (i.e., no model variation out of the great circle plane). The advantage of this technique is that the computation provides correct 3D geometric spreading, but because the computation is performed on a 2D grid one can attain higher frequencies than can be attained through a 3D approach. In this paper, radial component synthetic seismograms are computed for *SPdKS* with 6 second dominant periods; similar to those observed for this phase in broadband data. All synthetics are computed for a 500 km source depth.

When calculating synthetic seismograms for 1D ULVZ models, most studies have focused on the following ULVZ properties: (1) *S*-wave velocity reduction (δV_S), (2) *P*-wave velocity reduction (δV_P), (3) density increase ($\delta\rho$), and (4) ULVZ thickness (*h*). Thorne *et al.,* [2013b] added two new parameters when modeling ULVZs in 2D: (5) ULVZ length in the great circle arc direction (*length* measured in degrees), and (6) ULVZ position (Δ_{edge}). ULVZ position (Δ_{edge}) is defined as the angular distance from the source to the source-side edge of the ULVZ. For example, if we define the ULVZ *length* = 3° and Δ_{edge} = 10°, then the ULVZ starts at 10° away from the source and ends (Δ_{edge} + *length*) 13° away from the source. A summary of the model

space for which we calculate synthetic seismograms is shown in Table 3.1. In total we computed synthetic seismograms for 517 unique ULVZ models.

In order to examine geographic similarities in *SPdKS* waveform behavior, these data were first organized into 2.5° × 2.5° geographic bi ns based on location of the *Pd* inception points. For each geographic bin, we generated data stacks in 1° epicentral distance bins. We compared data to synthetics by cross-correlating each data stack with the appropriate distance synthetic seismogram for each of the 517 different ULVZ models. An average cross-correlation coefficient (CCC) was calculated for each model by averaging the CCC's for each synthetic-data stack pair in each model. Thus, we use a single number to describe the goodness of fit of each ULVZ model.

A consistent problem with modeling *SPdKS* waveforms is the significant tradeoffs between model parameters [*Garnero and Helmberger*, 1998]. Many models may explain the data equally well, yet, model parameters vary significantly. In addition to standard tradeoffs with velocity and thickness there are also trade-offs with ULVZ size and location. We computed a Welch's t-test, to compare the goodness of fit for each of the ULVZ models to the model with the highest mean CCC. For example, if the 95% confidence interval contains two models, then those models fit the data the same at least 95% of the time. In this way we can quantitatively compare which ULVZ models fit these data equally.

Table 3.1. ULVZ models computed for *SPdKS* analysis.

δV_S (%)	δV_P (%)	$\delta\rho$ (%)	*h* (km)	Length (deg)	Length (km on CMB)	Edge (deg)
-15	-5	+10	10, 15, 20, 30	1.5	91	10, 11.5, 13, 14.5, 16, 17.5, 19
-15	-5	+10	5, 10, 15, 20, 30	3	182	8.5, 10, 11.5, 13, 14.5, 16, 17.5, 19
-15	-5	+10	10, 15, 20	6	364	5.5, 7, 8.5, 10, 11.5, 13, 14.5, 16, 17.5, 19
-15	-5	+10	7.5, 10, 15, 20, 25	12	728	1, 2.5, 4, 5.5, 7, 8.5, 10, 11.5, 13, 14.5, 16, 17.5, 19
-30	-10	+10	10, 15, 20, 30	1.5	91	10, 11.5, 13, 14.5, 16, 17.5, 19
-30	-10	+10	5, 7.5, 10, 12.5, 15, 20, 30	3	182	8.5, 10, 11.5, 13, 14.5, 16, 17.5, 19
-30	-10	+10	7.5, 10, 15, 20, 30	6	364	5.5, 7, 8.5, 10, 11.5, 13, 14.5, 16, 17.5, 19
-30	-10	+10	7.5, 10, 15	12	728	1, 2.5, 4, 5.5, 7, 8.5, 10, 11.5, 13, 14.5, 16, 17.5, 19
-45	-15	+10	10, 15, 20, 30	1.5	91	10, 11.5, 13, 14.5, 16, 17.5, 19
-45	-15	+10	5, 7.5, 10, 12.5, 15, 20, 30	3	182	8.5, 10, 11.5, 13, 14.5, 16, 17.5, 19
-45	-15	+10	5, 7.5, 10, 15, 20	6	364	5.5, 7, 8.5, 10, 11.5, 13, 14.5, 16, 17.5, 19
-45	-15	+10	5, 7.5, 10, 15	12	728	1, 2.5, 4, 5.5, 7, 8.5, 10, 11.5, 13, 14.5, 16, 17.5, 19

CHAPTER 4

RESULTS

4.1 Coral Sea Region

Data for the Coral Sea region are shown in Figure 2.2a. All data traces are shown (gray) overlain with data stacks in 1° epicentral bins. These data stacks are shown overlain on synthetic predictions for the PREM model in Figure 2.2b. There are four traces at an epicentral distance of 112° that show distinctive ULVZ-like waveforms. That is, these traces (heavy black line at 112° in Figure 2.2b) show the *SPdKS* arrival is fully bifurcated from *SKS*, whereas in the PREM model (underlying gray traces in Figure 2.2b) *SPdKS* is just starting to emerge from the shoulder of *SKS*. The majority of these data are recorded at relatively long distances (116°-124°) over which the waveforms appear more PREM-like. Nevertheless, these data show a *SPdKS* delay with respect to PREM predictions of up to 4 s (at 124°) which is suggestive of ULVZ presence.

Comparisons of these data to a subset of synthetic predictions are summarized in Figure 4.1a. In general we find that ULVZ models with large angular size (e.g., *length* = 6° or 12°; top and bottom rows respectively) fit these data the best. The goodness of fit degrades significantly for models with smaller angular size (*length* = 1.5 ° or 3° not shown in Figure 4.1a). Synthetics for the best fit ULVZ model (red star indicates best-fit in Figure 4.1a, model parameters: δV_S = -15%, δV_P = -5%, *h* = 20 km, *length* = 12°, and Δ_{edge} = 11.5°) are shown overlain on data stacks in the first column of Figure 4.1b. Here we see the relative timing and amplitude of *SPdKS* with respect to *SKS* is well fit (avg. CCC = 0.877). However, inspection of Figure 4.1a shows that several models explain these data equally as well. The dashed black line is drawn around those models within the 90% confidence limit. For example, Figure 4.1b shows the model that fits these data

3rd overall (green star indicates 3rd best fitting model in Figure 4.1a, model parameters: δV_S = -45%, δV_P = -15%, *h* = 7.5 km, *length* = 12°, and Δ_{edge} = 4.0°) compared with data stacks (avg. CCC = 0.876). This model is shown as it represents a different class of ULVZ models (δV_S = -45%, δV_P = -15%), than the other best-fitting models (δV_S = -15%, δV_P = -5%). In comparing waveforms for these two models, there is little distinction between them, which exemplifies the strong modeling tradeoffs inherent in *SPdKS* data. Considering which models provide the best-fit (areas highlighted in blue in Figure 4.1a), we cannot distinguish between models with different V_P and V_S reductions. That is, models with δV_S = -45%, δV_P = -15% and δV_S = -15%, δV_P = -5% are equally capable of predicting the waveforms for these data. However, regardless of V_P and V_S reductions, models with angular sizes 6° ≤ *length* ≤ 12° provide an improved quality of fit over those models with smaller angular sizes. Additionally we find that the position of the ULVZ is most likely in the range 4° ≤ Δ_{edge} ≤ 13°, and that ULVZ thickness is in the range 10 km ≤ *h* ≤ 25 km. The tradeoff space is large in determining which ULVZ model best fits these data, nevertheless, strong evidence exists in this location for ULVZ presence. We indicate the position and size of the best-fitting ULVZ model for this region in Figure 2.1b (solid red box).

4.2 South and North Philippine Sea Regions

Data for the S. Philippine Sea region are shown in Figure 2.2c. All data traces are shown (gray traces) overlain with data stacks in 1° epicentral bins (black traces). These data stacks are shown overlain on synthetic predictions for the PREM model in Figure 2.2d. This region has excellent data coverage and shows remarkable similarity in waveform characteristics for each of our 2.5° × 2.5° geographic bins. Hence, for this analysis we grouped data for all geographic bins together. The data stacks (Figure 2.2d) are nearly identical to PREM predictions for all distances. Minor *SPdKS* delays are observed (< 1 s) at distances near 125°. The PREM model (avg. CCC = 0.884) or ULVZ models in which *SPdKS* almost entirely misses the ULVZ fits these data the best, and hence we see no indication of ULVZ presence in this region. Excellent data coverage also exists for the entire distance range in the N. Philippine Sea region. The waveforms are in

excellent agreement with PREM predictions and data/model comparisons (avg. CCC = 0.881) also indicates an absence of ULVZ presence.

4.3 South China Sea Region

There is less agreement in waveform characteristics for data sampling the S. China Sea region between our 2.5° geographic bins. Here we discuss these data in three groupings depending on *Pd*-inception point and azimuth of *Pd* arcs on the CMB (see Figure 2.1c: group *i* - red *Pd* arcs, group *ii* - purple *Pd* arcs, and group *iii* - green *Pd* arcs). Waveforms for group *i* show good agreement with PREM predictions for distances between 112°-125°. Some source complexity exists for one event, however traces from 110°-112° shows *SPdKS* emergence with amplitude larger than *SKS* which is not predicted by the PREM model. This waveform behavior is indicative of ULVZ presence [see, e.g., *Thorne et al.*, 2013b]. The group *ii* dataset is sparsely populated (20 total traces), yet these waveforms show a slight delay (roughly 2 s) of *SPdKS* for distances between 112° and 117° (no data exist at larger distances) which could indicate ULVZ presence. Group *iii* traces are also sparsely populated (25 total waveforms). In this grouping, two striking waveforms exist at a distance of 113° in which the *SPdKS* arrival is prominently emerging from the *SKS* arrival. Additionally these data show broadening (possibly due to multiple overlapping arrivals) in the distance range of 108°-110° which is indicative of *Pd*-inception inside a ULVZ [see e.g., *Thorne et al.*, 2013b].

Comparisons with synthetic predictions show that group *i* data are best explained by ULVZ models with small angular size (1.5° ≤ *length* ≤ 3°). Locations in the range 10° ≤ Δ_{edge} ≤ 11.5° also provide the best fits, indicating a small ULVZ may exist. The best fit model (avg. CCC = 0.875) has ULVZ characteristics: δV_S = -30%, δV_P = -10%, *h* = 5 km, *length* = 3°, and Δ_{edge} = 10.0°. The best fit model for group *ii* (avg. CCC = 0.841) is a ULVZ with characteristics: δV_S = -45%, δV_P = -15%, *h* = 5 km, *length* = 3°, and Δ_{edge} = 11.5°. For these data models with δV_S = -45%, δV_P = -15% and δV_S = -30%, δV_P = -10% provide the best fit. Models with δV_S = -15%, δV_P = -5% show a degraded fit. There is a distinct bulls-eye pattern in the CCC analysis characterized by ULVZ thickness in the range 5 km ≤ *h* ≤ 15 km; angular size 1.5° ≤ *length* ≤ 3°,

and position $8.5° \leq \Delta_{edge} \leq 10°$. The comparisons between model and data for g roup *iii* data are virtually identical to those data for group *ii*. These data suggest the presence of at least one small-scale ULVZ in each data grouping. Our inferred ULVZ locations are displayed in Figure 2.1c.

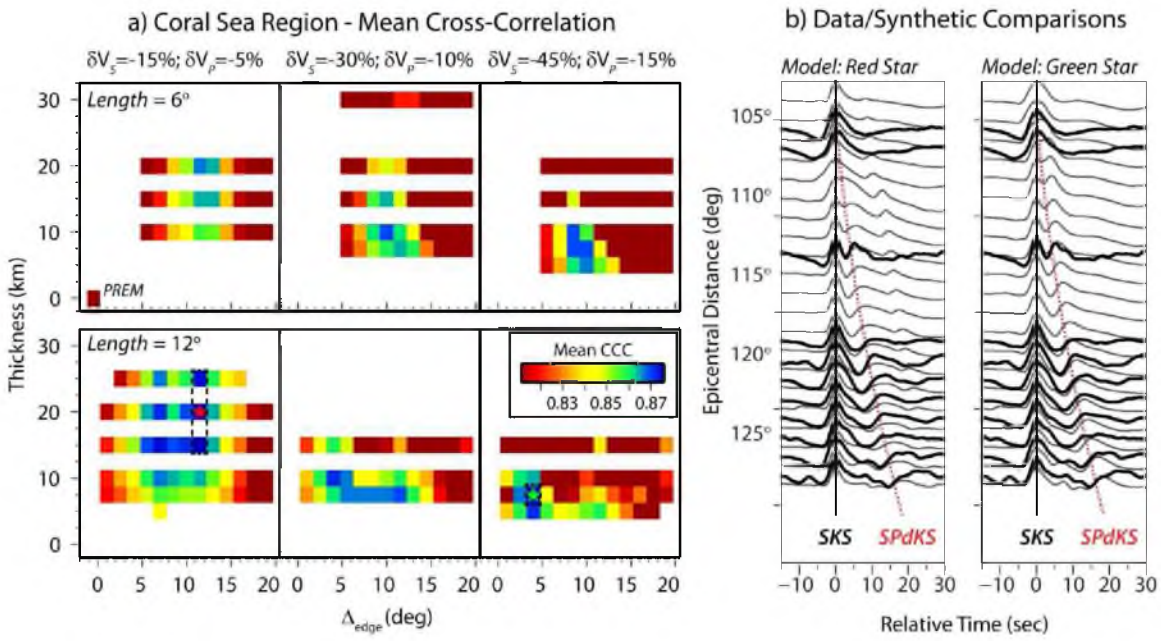

Figure 4.1. Modeling results for the Coral Sea region. (a) The mean CCC between data and synthetic models for the Coral Sea Region is shown. The top and bottom rows are for models with *lengths* = 6° and 12° respectively. Each column is for dif ferent values of δV_S and δV_P (e.g., column 1 has δV_S=-15%, δV_P=-5%). In each row and column the average CCC is shown (scaled from red through blue) based on ULVZ thickness (*h*) and angular position (Δ_{edge}). The average CCC for the PREM model is shown in lower left corner of the first plot. The best fitting model is indicated by the red star (synthetics shown in panel b), and the third best-fitting model is indicated by the green star (synthetics shown in panel b). The dashed black line shows models within the 95% confidence limit for explaining these data equally well. (b) Comparison of data stacks (black traces) with synthetic seismograms (gray traces) for two models. Model 1 is the best-fit model with ULVZ parameters: δV_S=-15%, δV_P=-5%, *h* = 20 km, *length* = 12°, and Δ_{edge} = 11.5°. Model 3 is the 3rd best-fitting model with ULVZ parameters: δV_S=-45%, δV_P=-15%, *h* = 7.5 km, *length* = 12°, and Δ_{edge} = 4.0°. Radial component displacement seismograms are shown aligned and normalized to unity on the *SKS* arrival. The dashed red line shows the approximate *SPdKS* arrival time.

CHAPTER 5

DISCUSSION AND CONCLUSIONS

From our analysis of *SPdKS* data, we see no evidence of ULVZs in the N. and S. Philippine Sea regions. Previously *Idehara et al.,* [2007] examined these regions with *ScP* data. Although only a handful of *ScP* observations have been made in this region, the *ScP* bounce points that overlap our *Pd* arcs are consistent with our conclusion that no ULVZ exists in these areas. *Idehara et al.,* [2007] and *Idehara* [2011] both indicate the presence of a ULVZ 175 km to the southwest of our N. Philippine Sea data which is not sampled by our data.

ULVZs have been indicated in the Coral Sea region by multiple studies using the seismic phase *ScP* [*Rost and Revenaugh*, 2001; 2003; *Rost et al.*, 2010; *Rost et al.*, 2005]. These studies indicate that one or more ULVZs exist in this region with a thickness (*h*) averaging 9 km, with inferred P-wave velocity reductions from 5 to 8% and S-wave velocity reductions from 22 to 25%. From these previous studies, it is not possible to constrain the full dimensions of the ULVZ(s) in this region as there is incomplete *ScP* bouncepoint coverage (see Figure 2.1b). Our findings are consistent with ULVZ presence in this area; however our waveforms are indicative of a larger scale ULVZ (see Figure 2.1b). Our best-fitting model indicates a large ULVZ on the order of 700 × 700 km. Our inferred ULVZ position and size span the area in between ULVZ sightings from *ScP* data, suggesting that a single large ULVZ exists here. Some of the *ScP* data for this region display multiple postcursors, which is indicative of multipathing and consistent with the interpretation that the *ScP* observations are sampling the edge of this ULVZ. Our best-fit ULVZ model suggests a larger thickness (~20 km) than previously found for this region from *ScP* data (~9 km). We cannot rule out a thinner ULVZ as inspection of Figure 4.1a shows that a thin ULVZ

is also consistent with our *SPdKS* data (δV_S = -30%, δV_P = -10%). Regardless of ULVZ thickness, a large ULVZ (on the order of 12°) is required to match the *SPdKS* data. The discrepancy found for the thickness of the ULVZ may indicate that the *ScP* data are sampling thinner ULVZ edges, with the ULVZ thickening to up to 20 km in the center.

The South China Sea region has been probed in one study [*Idehara et al.*, 2007]. The results from this study indicate sporadic observations of ULVZ presence (see Figure 2.1b) but may indicate that two or three small-scale ULVZs exist in this region. *Idehara et al.,* [2007] modeled the amplitude ratio of the postcursor phase ScSP (an ScS wave that converts to a P-wave as it exits the ULVZ) relative to *ScP* which is sensitive to the *S*-wave velocity contrast. They conclude that δV_S reductions must be greater than 20% to account for the large amplitude ScSP postcursors observed, with the majority of their observations best fit with 30-40% *S*-wave velocity reductions. *SPdKS* data for our first group (red shaded box labeled *i*, Figure 2.1c) show the possible existence of a small ULVZ. This is not co-located with any previously observed ULVZ, but due its small size (*h* = 5 km, *length* = 3°) it may have been challenging to detect from single *ScP* observations. Our second data grouping (purple shaded box labeled *ii*, Figure 2.1c) shows a ULVZ in the vicinity of where *Idehara et al.,* [2007] have also inferred ULVZ presence. Although our *Pd* arcs may cross into another ULVZ to the northwest of our modeled ULVZ, our data are best-fit with the ULVZ as shown. This region is complex and may possibly include the interaction of 1 or 2 distinct small scale ULVZs. Our data are consistent with a ULVZ with a ~30% decrease in S-wave velocity and indicate that we likely have a thin (*h* < 10 km) and laterally small (*length* ≤ 3°) ULVZ. Our final data grouping (green shaded boxes, labeled *iii*, Figure 2.1c) shows the most direct evidence for ULVZ with *SPdKS*. In this region, we show two ULVZs. The ULVZ shown to the southeast indicates our best-fitting model. Data at short distances (< 110°) are indicative of a direct hit of *Pd*-inception points within a ULVZ due to the existence of a *SPdKS* precursors [*Thorne et al.*, 2013b], and suggest this ULVZ is located precisely where we have drawn it. The two anomalous waveforms we observed at a distance of approximately 112° are also indicative of a ULVZ and provide the basis for which we added the second ULVZ (green shaded box with dashed border). This ULVZ position does not come from our overall modeling of these data but

instead is drawn in as a possible ULVZ due to the two distinctive ULVZ waveforms observed in this data grouping. Hence, we emphasize that a ULVZ may also be present in this general region. Neither of these ULVZs have been indicated in previous studies. Overall, the S. China Sea region is the most complex area we have studied and appears to contain several small scale ULVZs which should be targeted by future high resolution *ScP* studies.

It is important to note that in this study we have only compared *SPdKS* data to synthetic seismograms computed for 3:1 V_S to V_P velocity reductions. Many studies [e.g., *Revenaugh and Meyer*, 1997; *Rost et al.*, 2005] have demonstrated that waveforms are consistent with this 3:1 velocity reduction. However, there is evidence to support 1:1 or 2:1 ratios for ULVZs located in the central Pacific [e.g., *Zhang et al.*, 2009]. Nevertheless, we do not include these velocity ratios in this study due to the large computational time required to generate 2.5D synthetic seismograms at these frequencies. Future efforts should consider ULVZs with 1:1 and 2:1 V_S to V_P velocity reductions.

We collected a new data set of broadband *SPdKS* recordings examining these data for presence/nonpresence of ULVZs. We found that data collected in the N. and S. Philippine Sea region are devoid of ULVZ characteristics. However, the S. China Sea and Coral Sea regions show evidence of ULVZ presence. The Coral Sea region may contain a relatively large scale ULVZ (on the order of 700×700 km). The S. China Sea region is characterized by multiple small scale ULVZs (approximately 180×180 km). We compared our modeling results to previous studies using short period *ScP* data. Both data sets are in agreement on the existence or non-existence of ULVZs in this area. Due to strong modeling tradeoffs in *SPdKS* data, it is useful to combine these data sets because when using these in conjunction we can gain greater insight into ULVZ locations as well as reduce the uncertainty in ULVZ elastic parameters.

APPENDIX

SUPPLEMENTARY MATERIALS

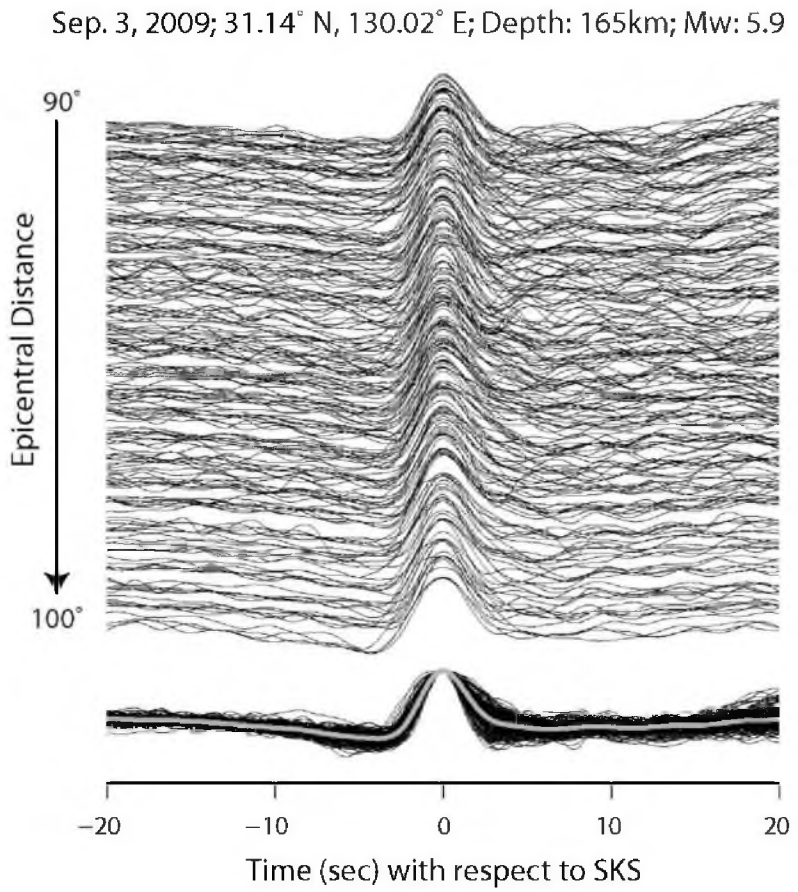

Figure A.1. A source-time function created from a broadband waveform stack on *SKS*. *SKS* data were gathered for an epicentral distance range of 90° to 100°. These data were examined visually to discard records with a poor SNR, and where *SKKS* and *Sdiff* were unrecognizable. Each event's remaining data were then stacked to create a source-time function to determine if the source is a clean impulse. *SKS* data with an epicentral distance range of 100° to 125° were then collected for events with a clean source. Hypothetical *Pdiff* for *SPdKS*/*SKPdS* are shown in Figure A.2.

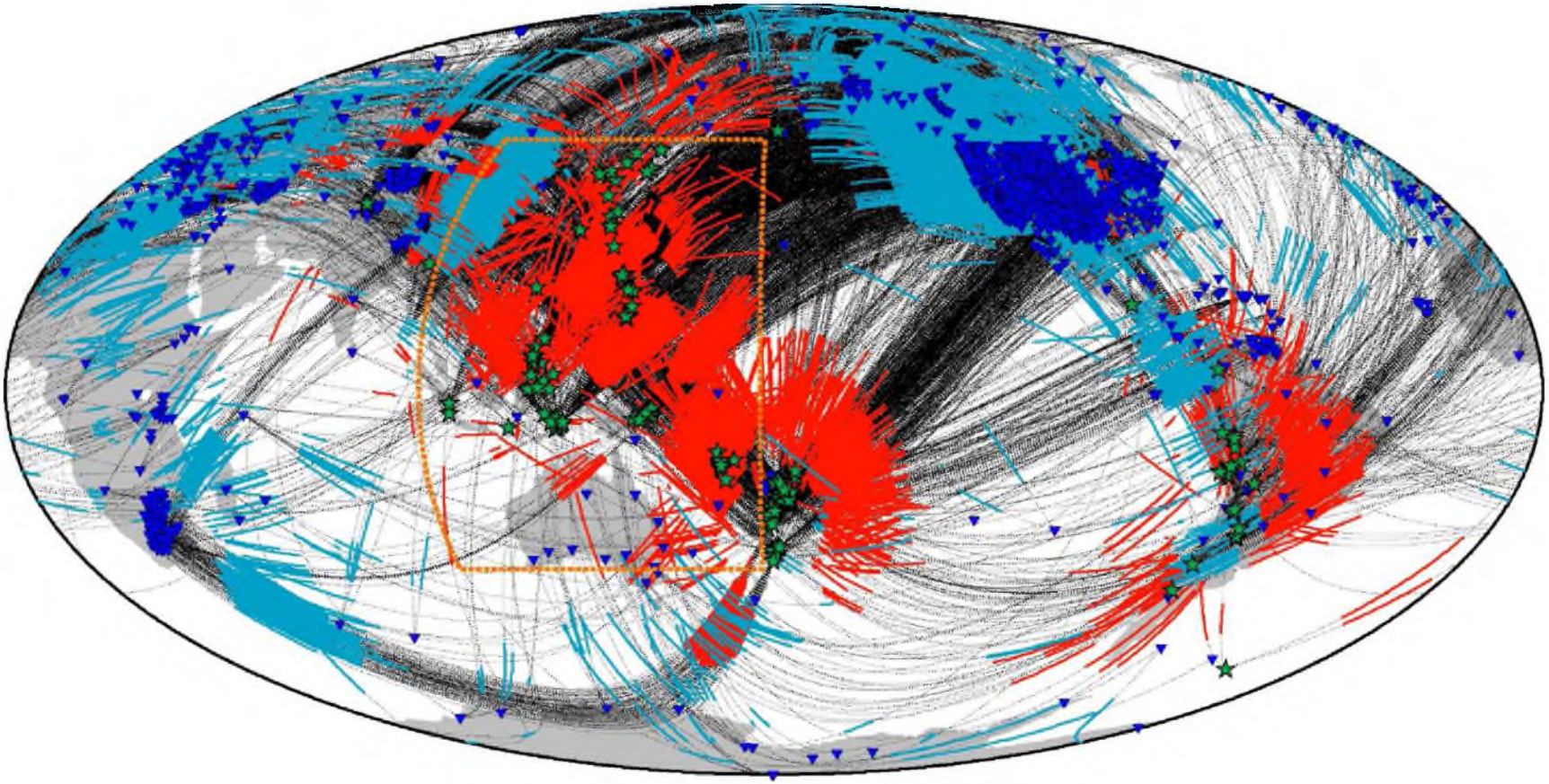

Figure A.2. Initial collection of broadband *SPdKS* data. Data are shown by *Pd* paths of *SPdKS* (red lines) and *SKPdS* (light blue lines) recorded at 1704 receivers (blue triangles), originating from 217 earthquakes (green stars).

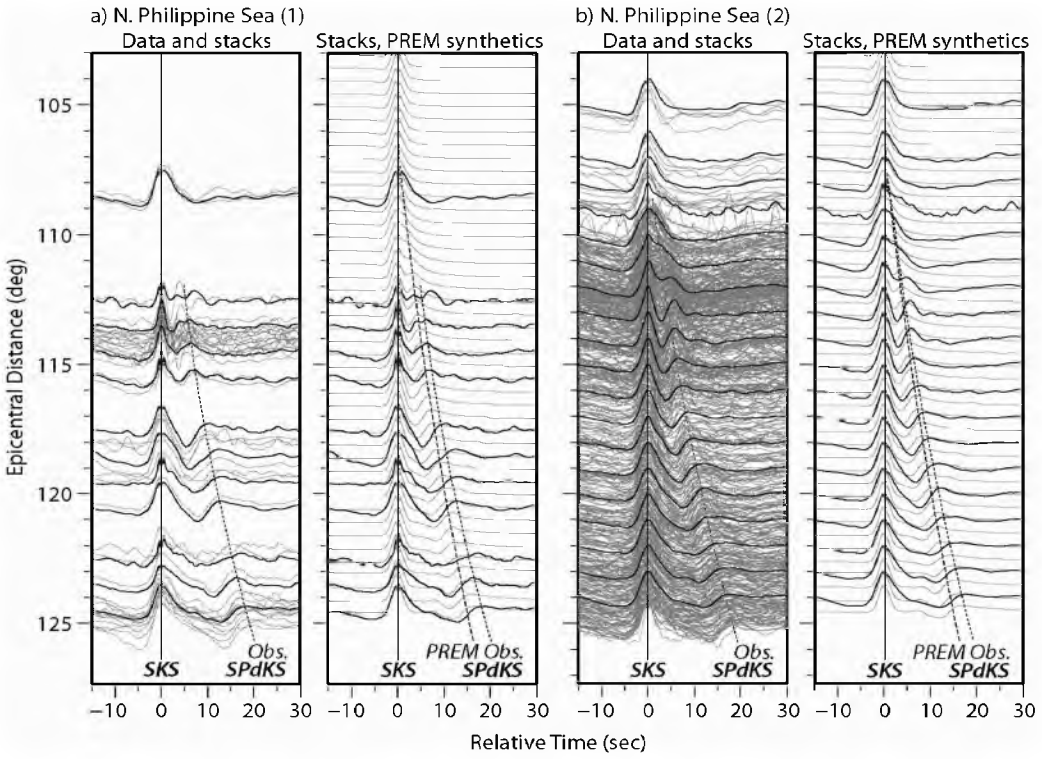

Figure A.3. Data observations for six of the eight bins. a) Data observations and comparison to PREM for the N. Philippine Sea (1). In the left profile the radial component seismograms (gray traces) are aligned on *SKS* showing the observed travel-time of *SPdKS* with stacks (black traces) overlaying them. The right profile shows PREM synthetics overlain by data stacks, both aligned on *SKS*. The PREM synthetic and observed arrivals of *SPdKS* are marked. b) Same as a) but for the N. Philippine Sea region (2). c), d), e), and f) are for the N. Philippine Sea (3), S. China Sea (1), S. China Sea (2), and S. China Sea (3) respectively.

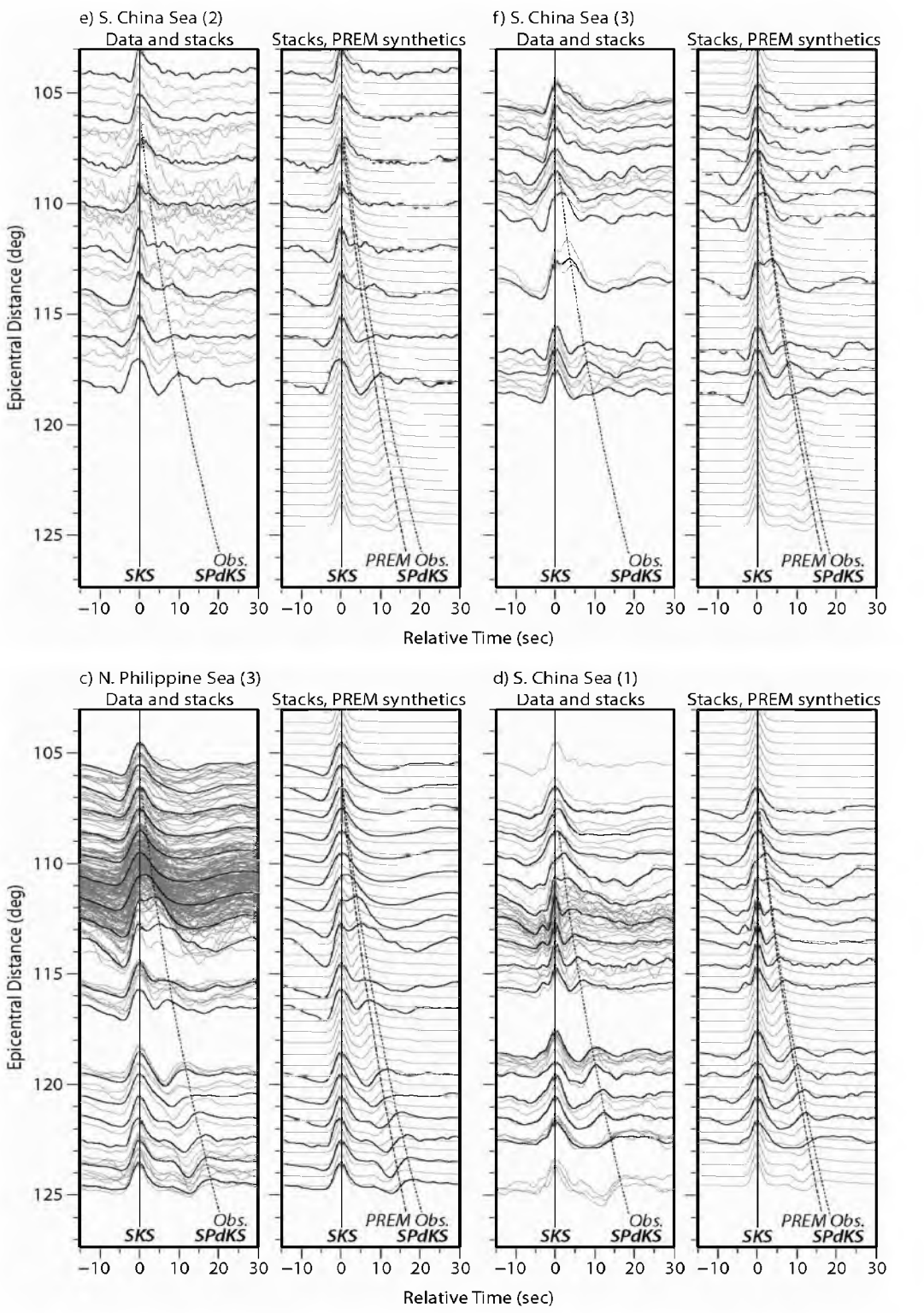

Figure A.3. continued

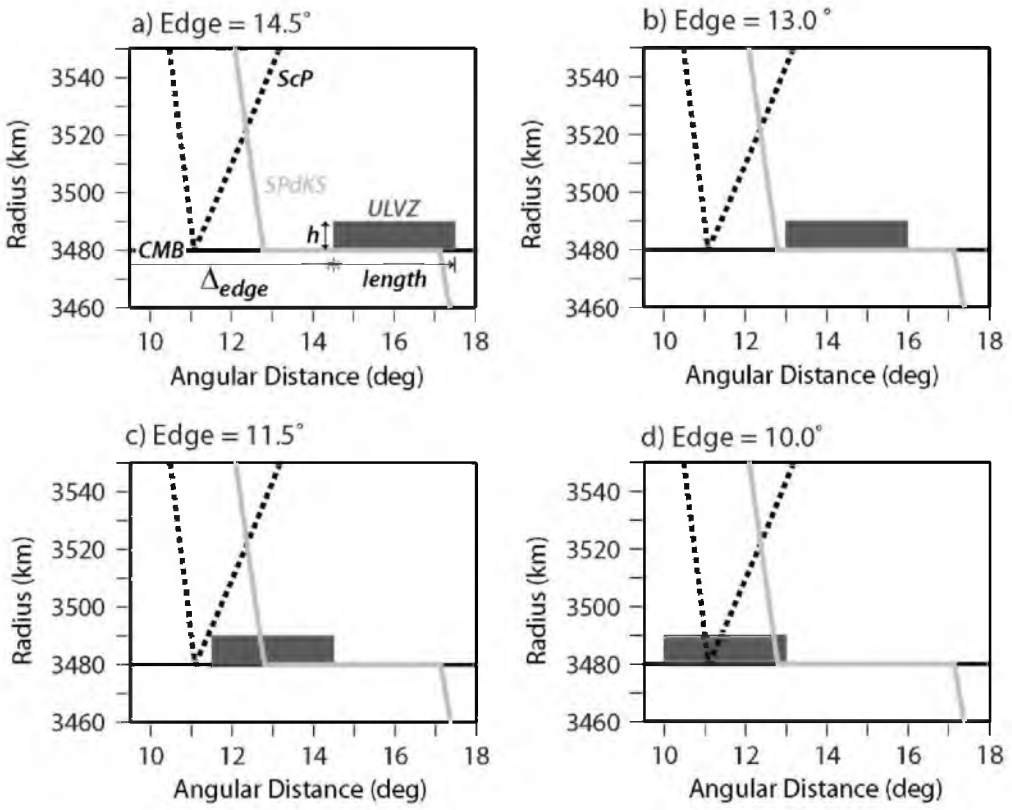

Figure A.4. 2D ULVZ model spatial properties. In each panel the ULVZ is shown as the gray shaded box, the *ScP* ray path for an epicentral distance of 40° is shown as the dashed black line, and the *SPdKS* ray path for an epicentral distance of 108° is shown with the light gray line. Ray paths are shown for a 500 km source depth. 2D ULVZ parameters are shown in panel (a). These parameters are: thickness (*h*), length in the great circle arc direction (*length*), and position of the leading edge of the ULVZ (Δ_{edge}). In panel (a) the parameters are *h*=10 km, *length*=3°, and Δ_{edge} =14.5°. Each panel shows a different ULVZ location used in our modeling: (a) Δ_{edge} = 14.5°, (b) Δ_{edge} = 13.0°, (c) Δ_{edge} = 11.5°, (d) Δ_{edge} = 10.0°

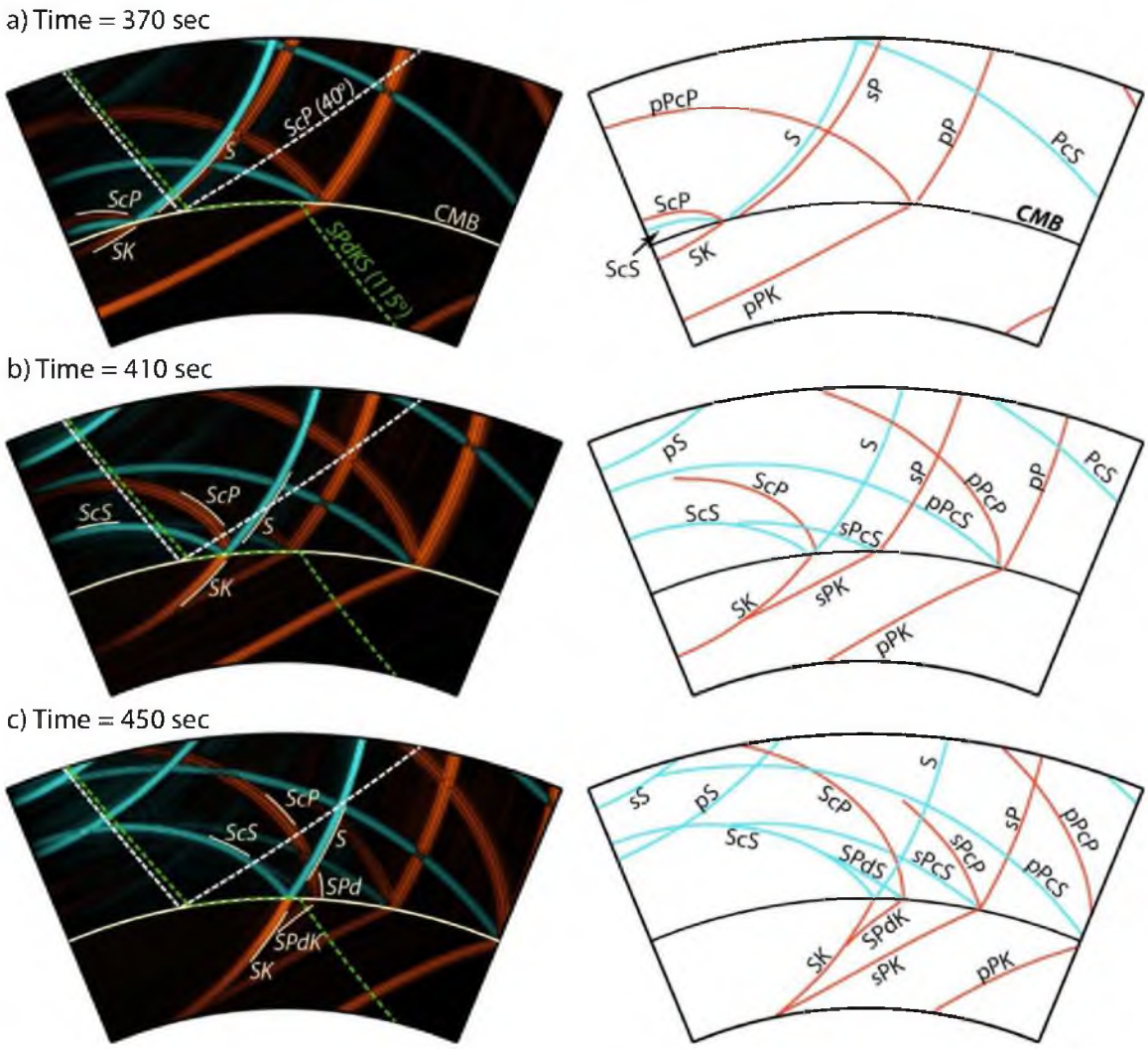

Figure A.5. A wave field that shows compressional (divergence; red lines) and shear (curl; blue lines) wave energy at three snapshots in time, a) 370 seconds, b) 410 seconds, and c) 450 seconds resulting from a seismic source 500 km in depth. The evolution of *ScP* (white dashed line) and *SPdKS* (green dashed line) waveforms can be seen going from a) to c) in the left column of the figure. The right column shows the relationship of all phases interacting with the area during the propagation of the wave field.

Figures A.6 – A.13 show the results of 517 ULVZ models compared by a) the mean of data stack CCCs, on a scale from zero to one with one being the best. The figures are separated into 12 plots based on seismic velocity decrease and length of the ULVZ in degrees. The top labels (S#/P#) represent the seismic phase and the percent decrease of that seismic phase's velocity through a ULVZ with a certain thickness (y-axis), edge (x-axis), and length (right side label; L#). Each model has a density increase of 10%, so the main control of seismic velocity decrease would be the fraction of partial melt in the ULVZ. Best models are a blue hue trending to red as the fit between the models and data stacks decrease. The color scale is saturated to brownish-red below the cutoff mean correlation shown as the minimum on the color bar of each figure. The top five models are marked with a star (red=best-fit, orange=2nd, green=3rd, cyan=4th, gray=5th). The PREM model is in the bottom left corner of the top left box. b) shows the percent confidence of a Welch's t-test when all the models are compared to the model with the highest mean. All models with a percent confidence under 10 are saturated to brownish-red. Parameters in b) are the same as a).

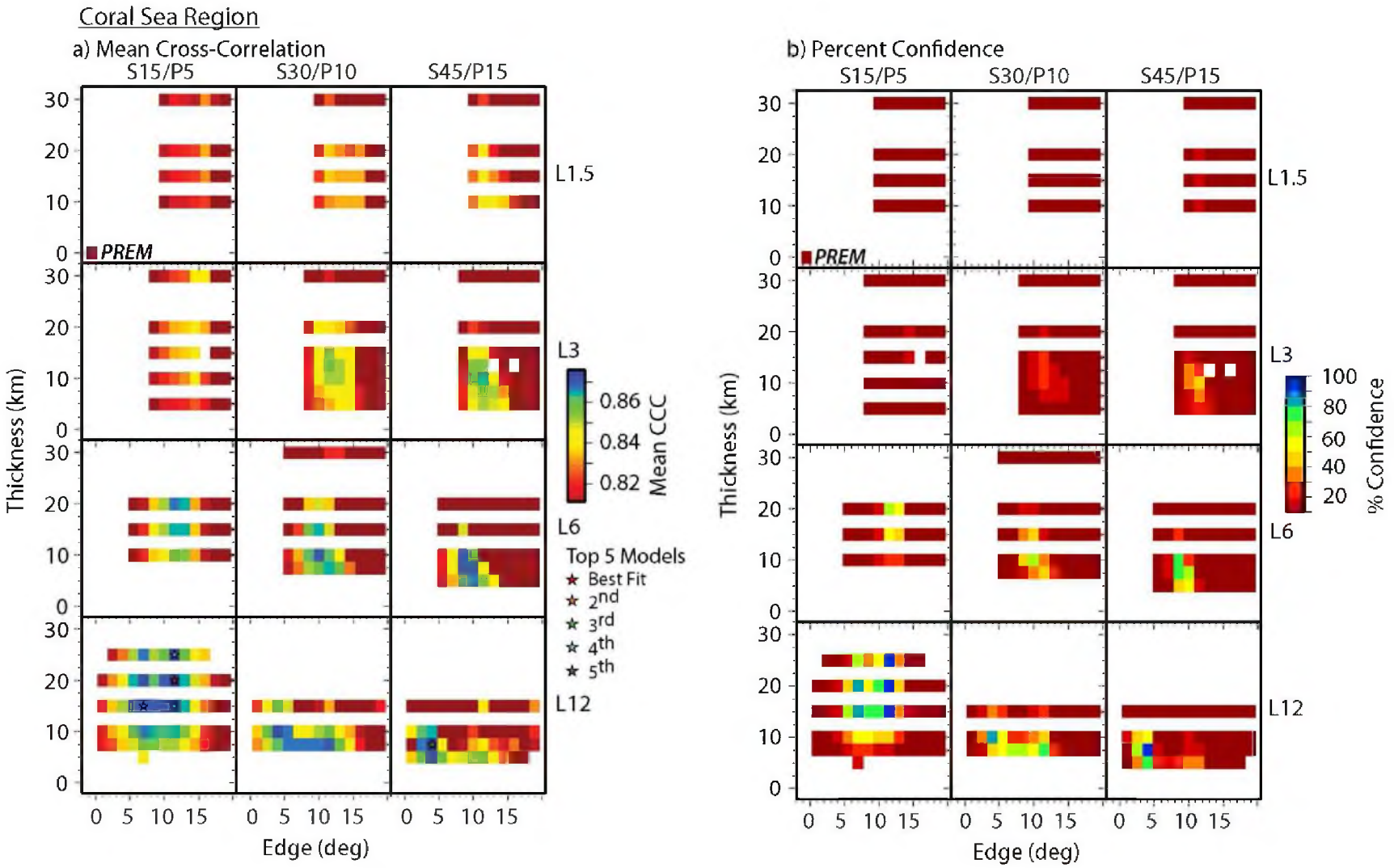

Figure A.6. Coral Sea Region

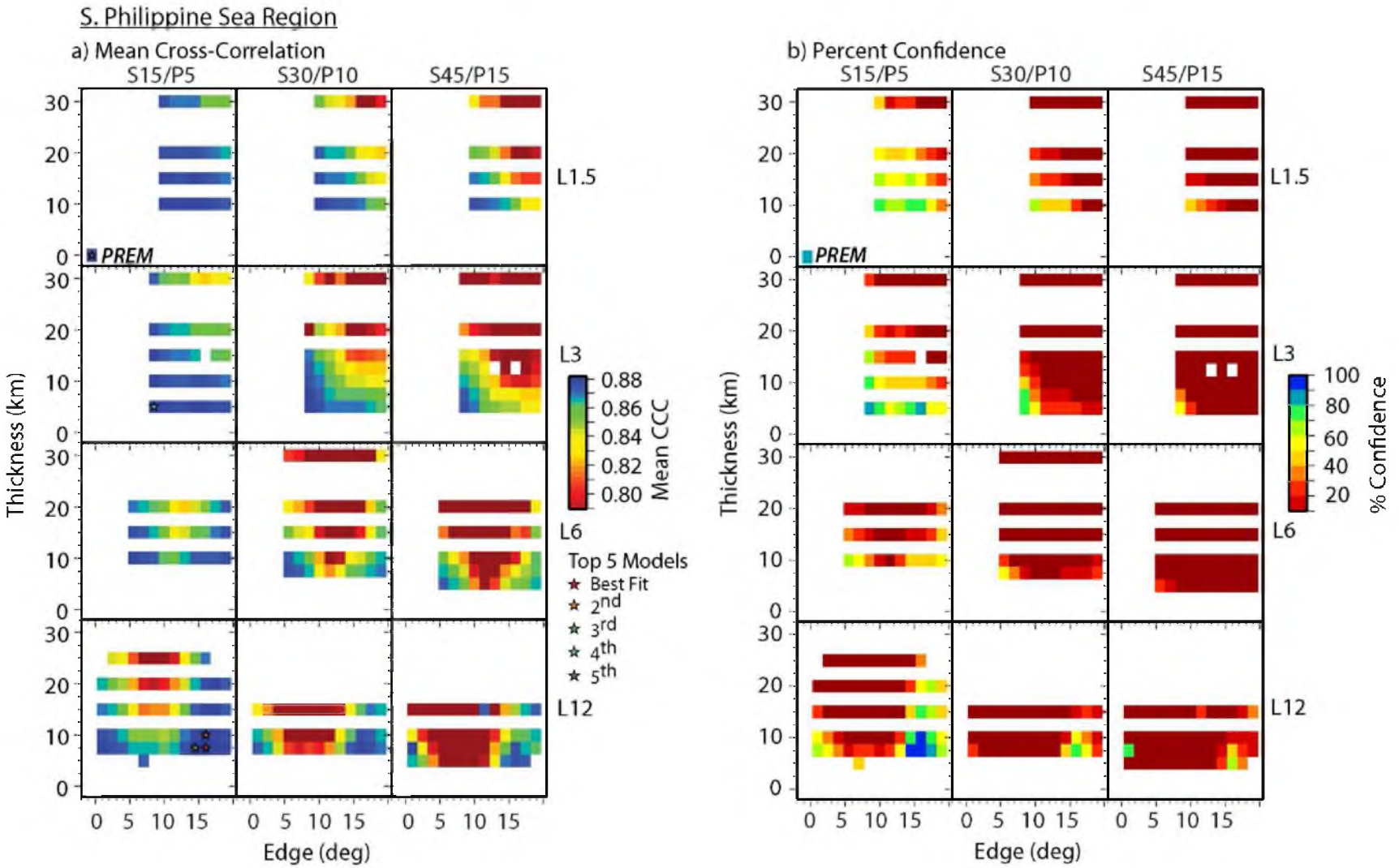

Figure A.7. S. Philippine Sea Region

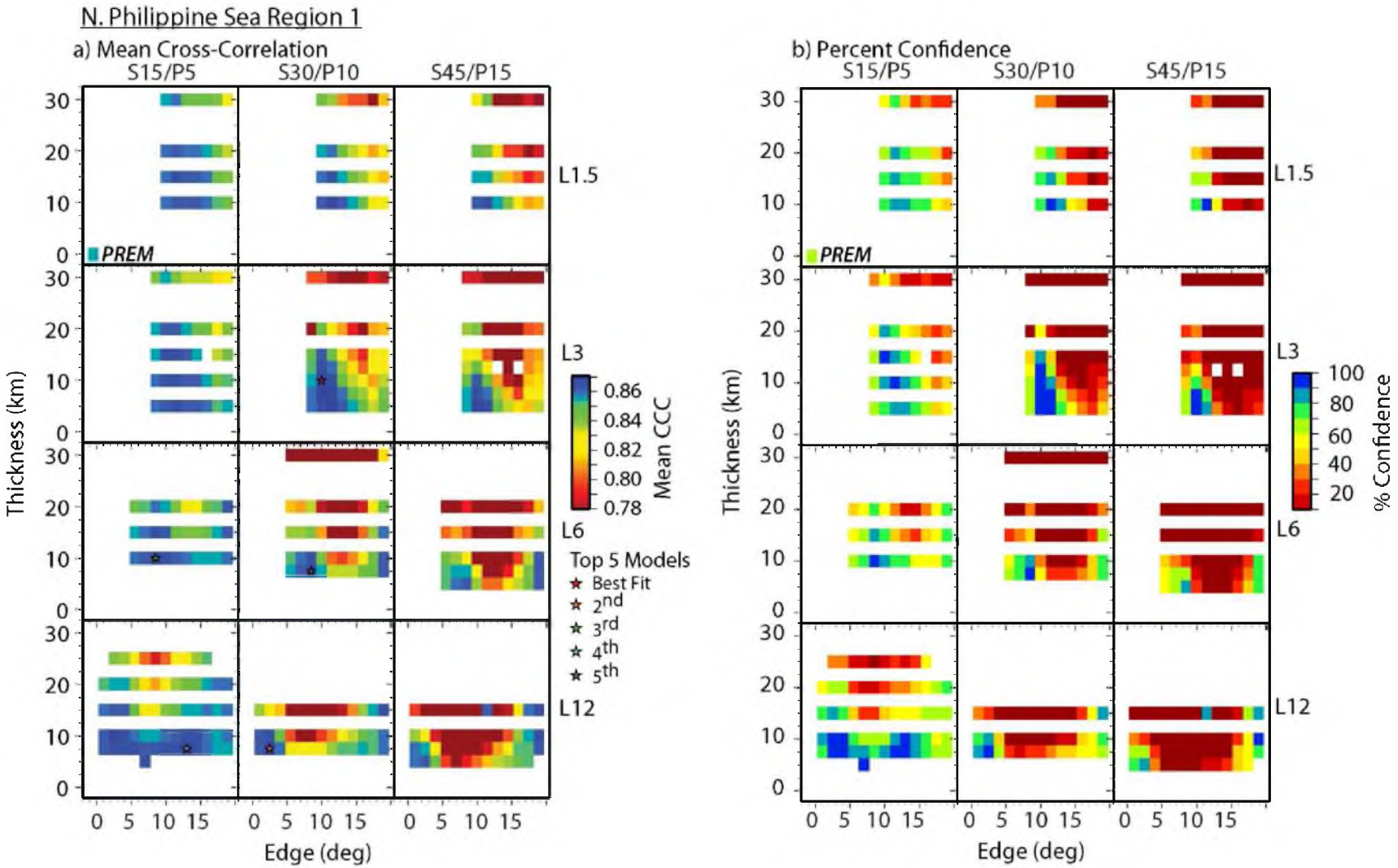

Figure A.8. N. Philippine Sea Region 1

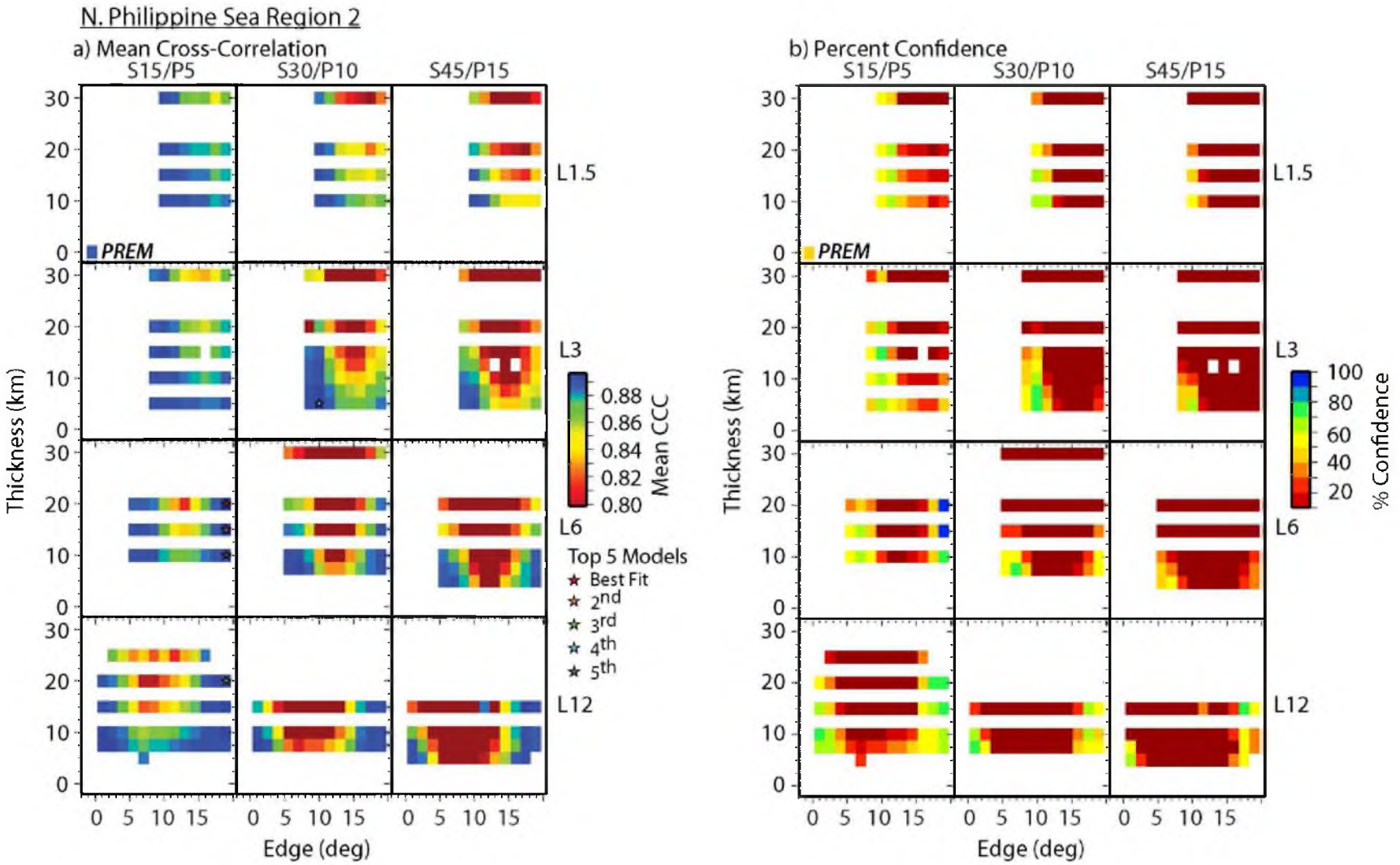

Figure A.9. N. Philippine Sea Region 2

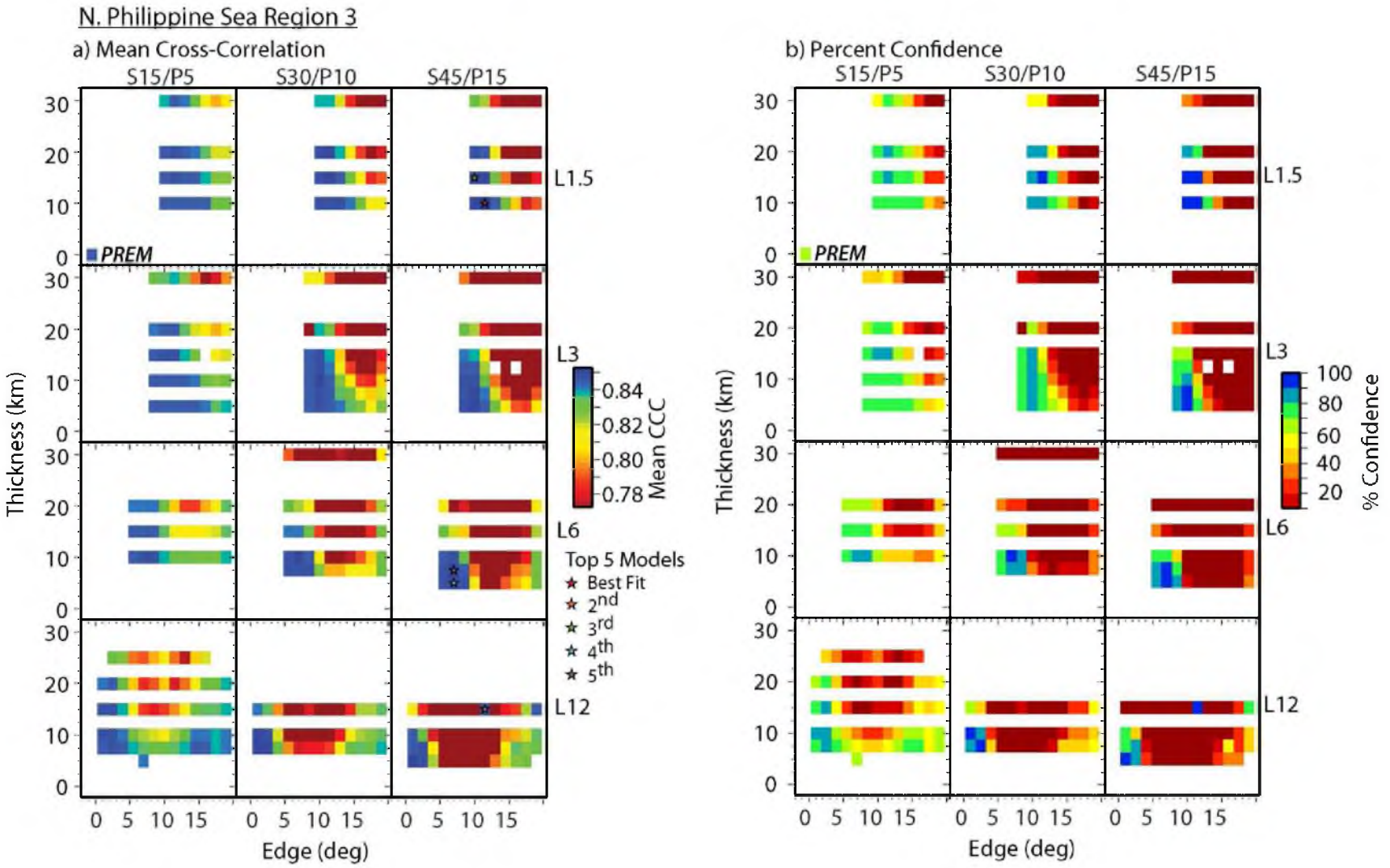

Figure A.10. N. Philippine Sea Region 3

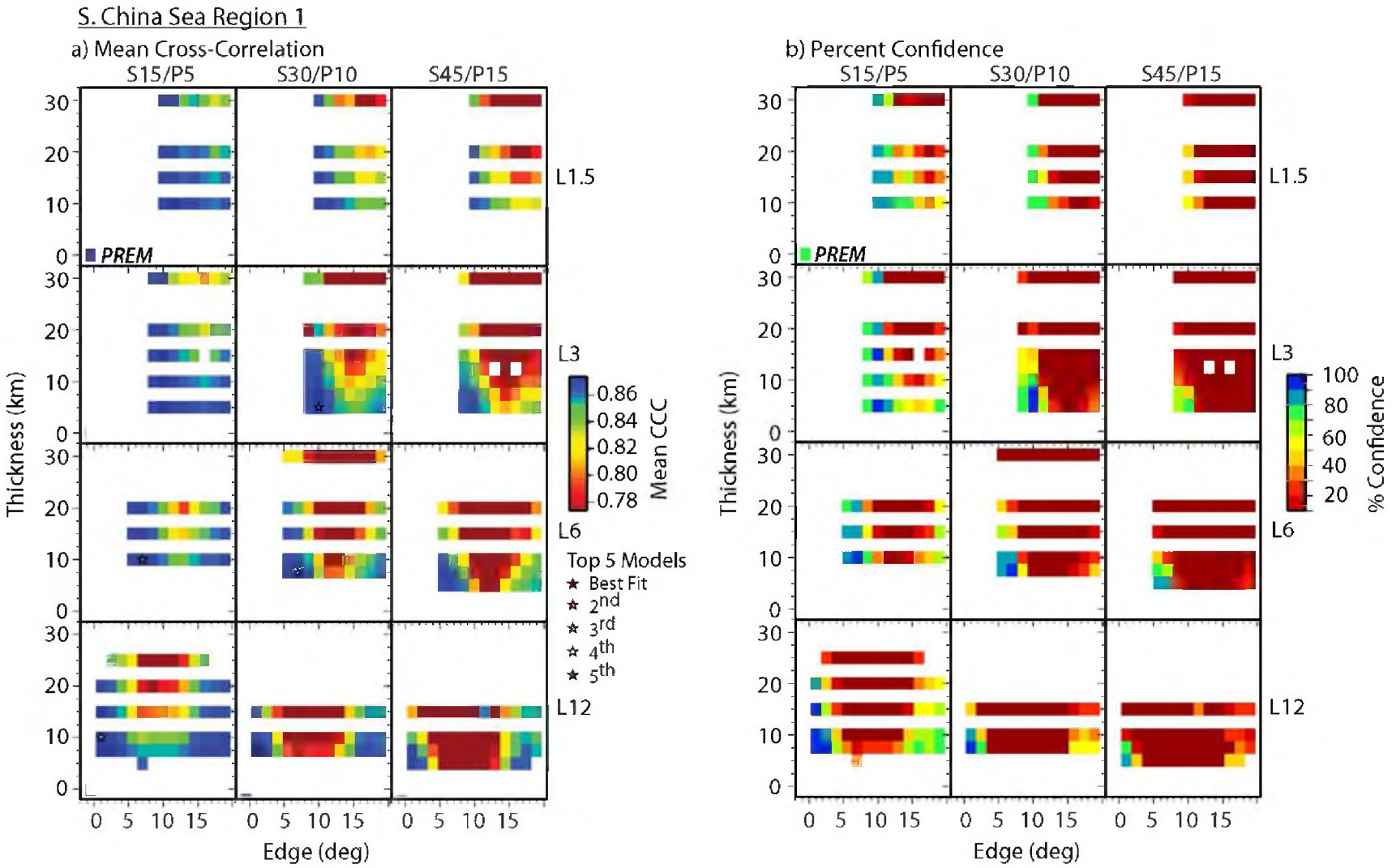

Figure A.11. S. China Sea Region 1

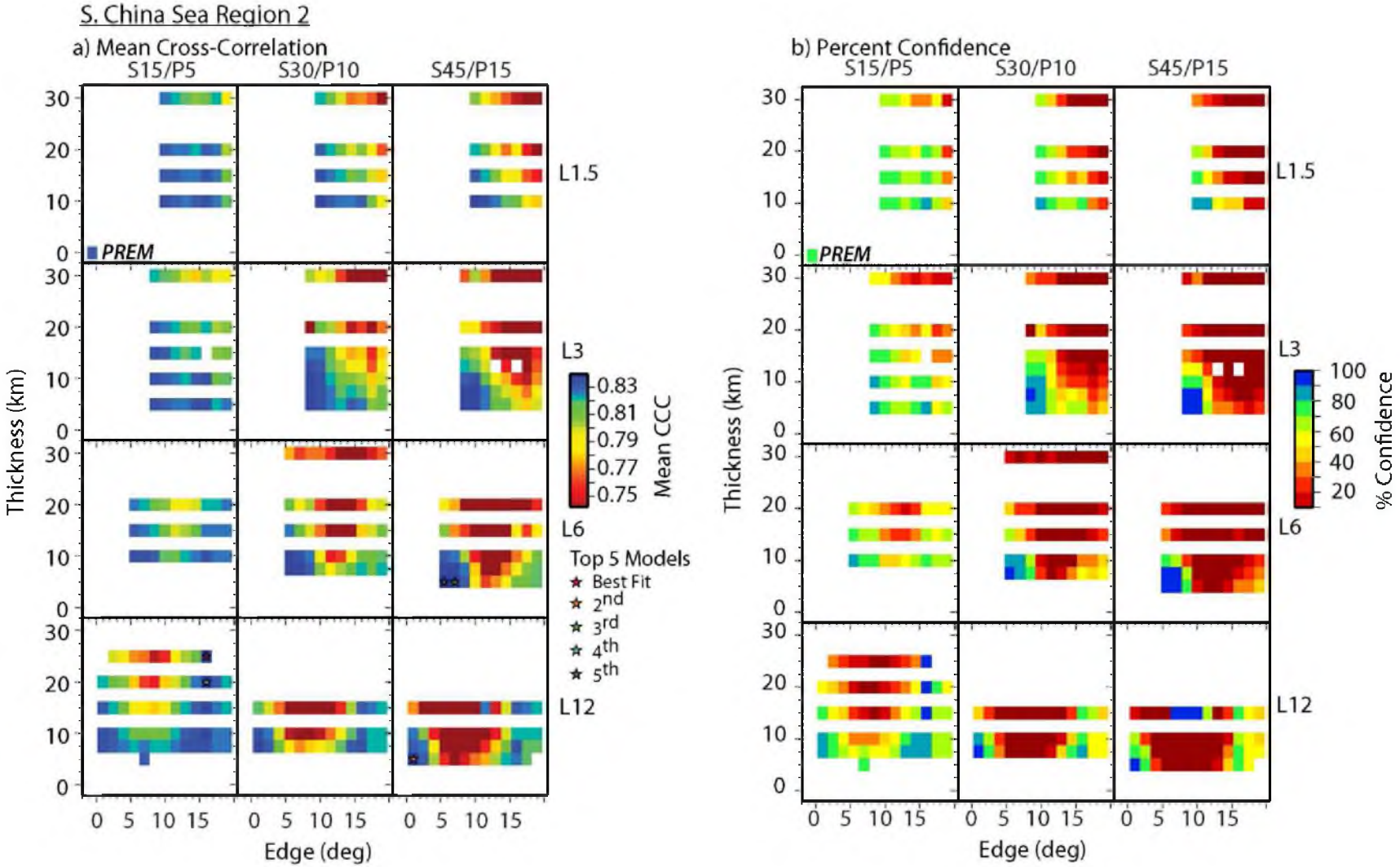

Figure A.12. S. China Sea Region 2

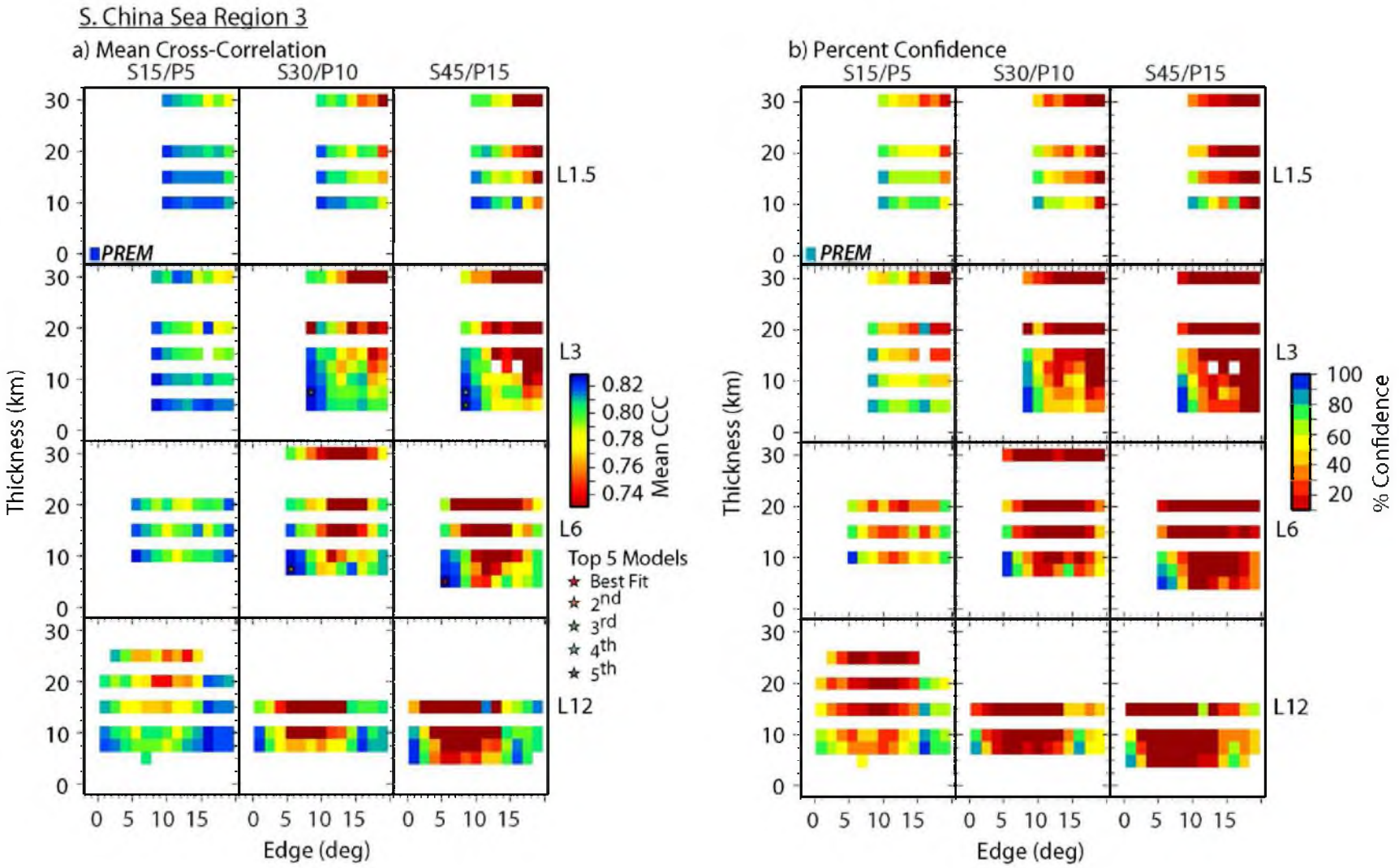

Figure A.13. S. China Sea Region 3

Figures A.14 – A.21 overview the five best-fit models for each region according to group cross-correlation means. a) Seismic profiles containing ULVZ model synthetics overlain by data stacks aligned on *SKS* (time equals zero) with observed moveout of *SPdKS* (dotted red line) relative to *SKS*. The parameters for each model are given at the top of each distance profile use the notation for each model as given by the following example: δV_S = -15%, δV_P = -5%, $\delta\rho$ = +10%, *thickness* = 20 km, *length* = 12°, and *Edge* = 11.5° equals S15/P5/ ρ10/h20/L12/E11.5. b) Map showing possible ULVZ location with respect to *Pd* segments. The boundary of the each region is the thick dashed line and the boundary of the each sub-bin is the thin dashed line. c) Ray path geometry showing interaction of *SKS* (blue line) and *SPdKS* (red line) with a 2D ULVZ (dark yellow box) at an epicentral distance of 109° for each of the five best-fit models.

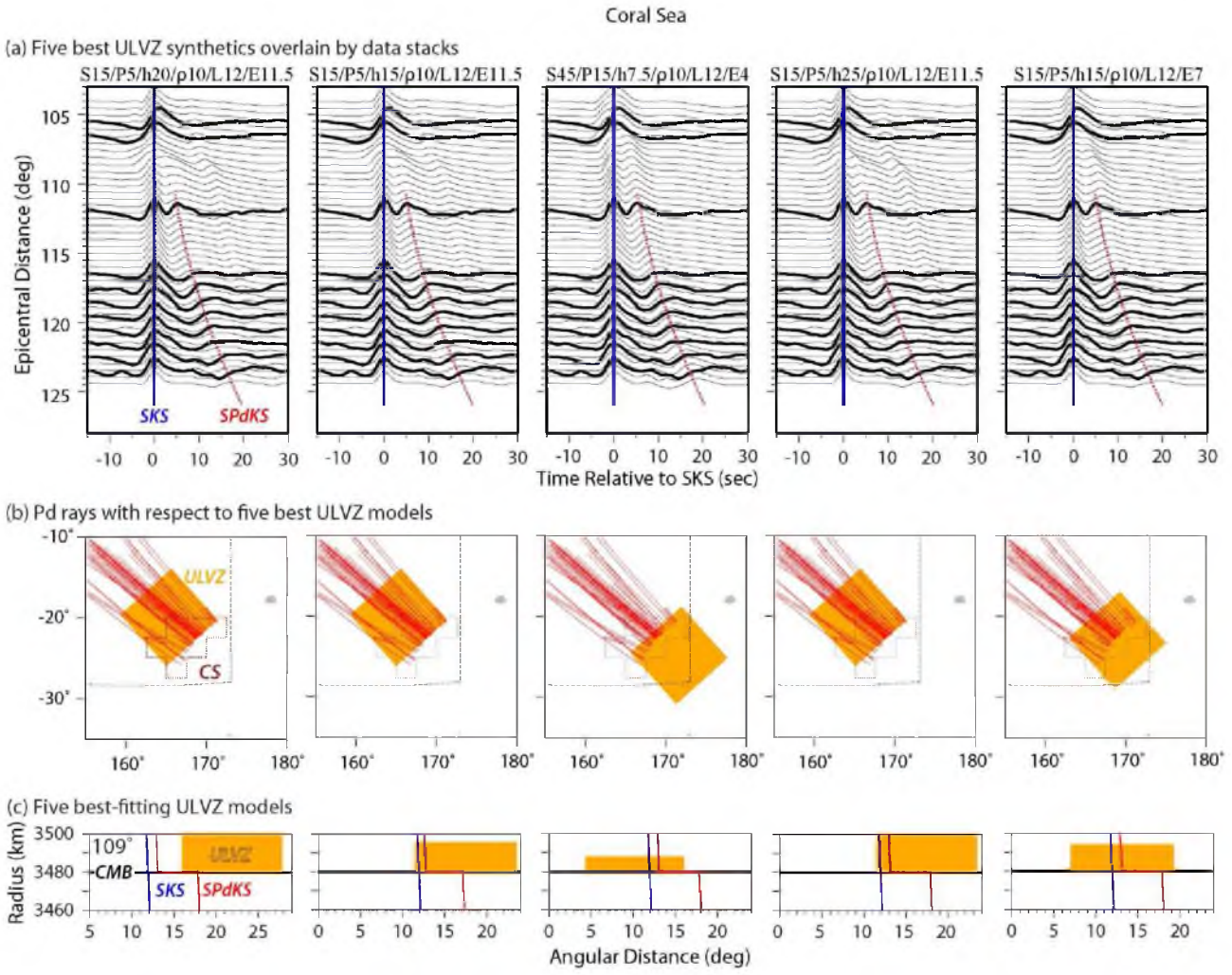

Figure A.14. Coral Sea Region

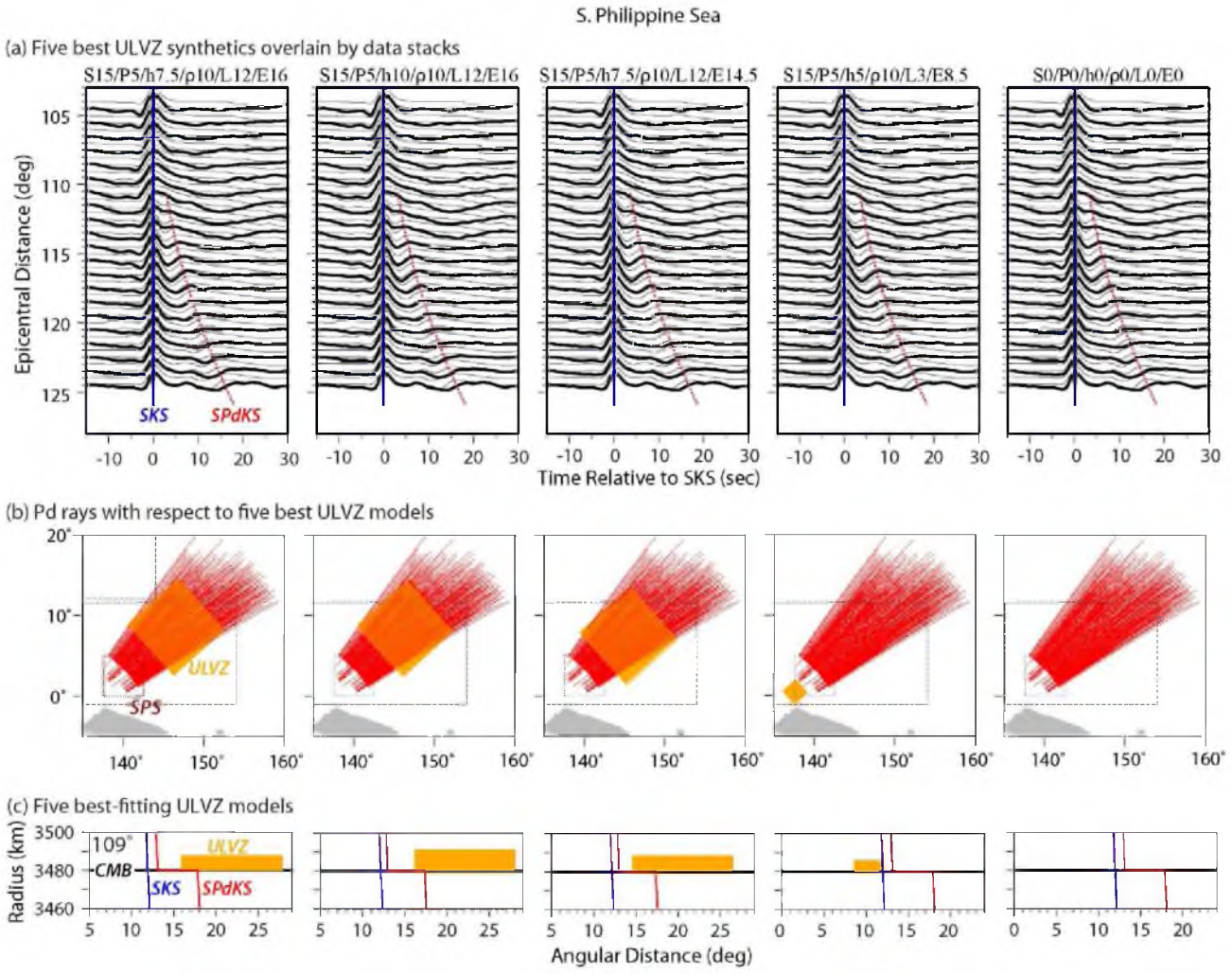

Figure A.15. S. Philippine Sea Region

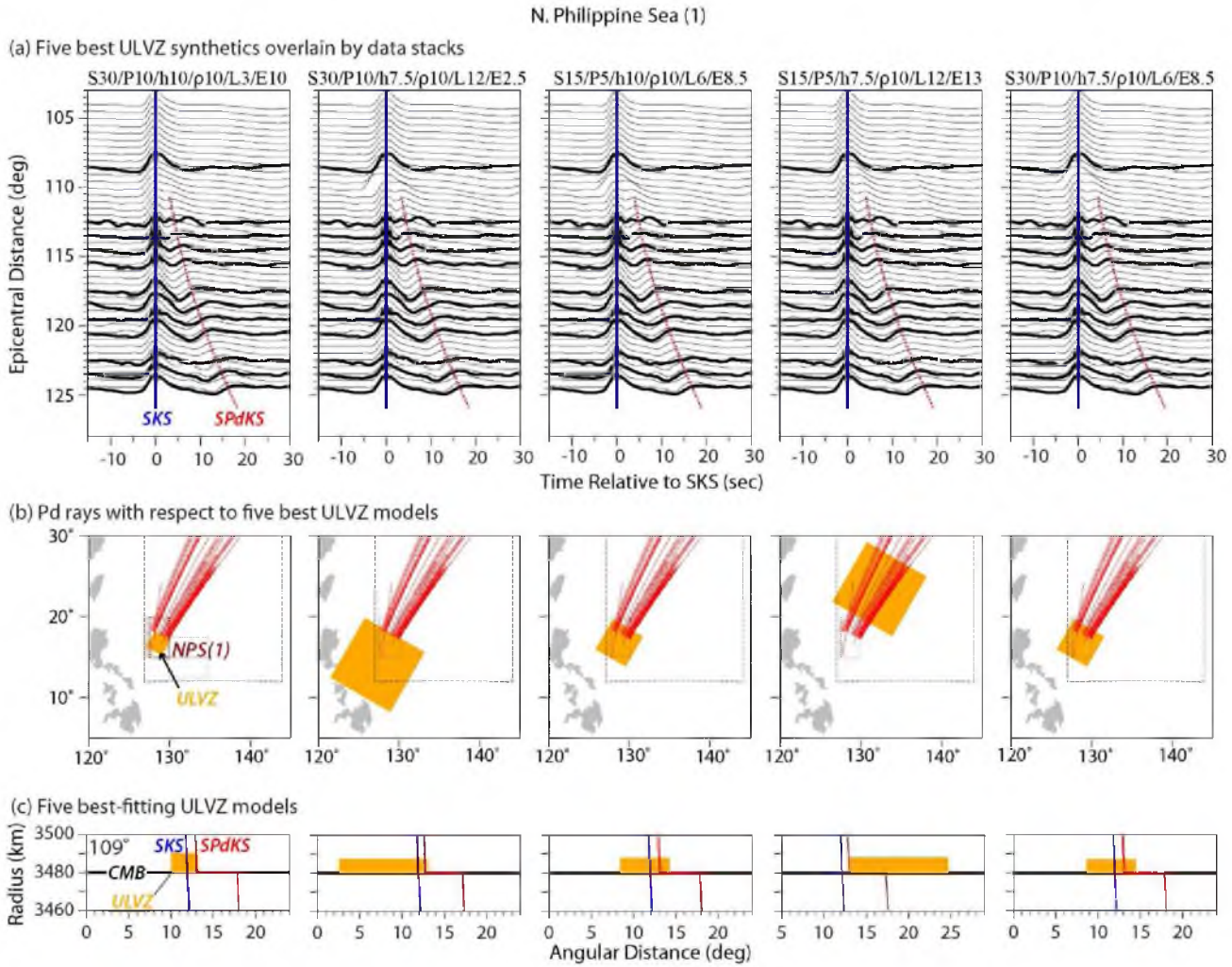

Figure A.16. N. Philippine Sea Region 1

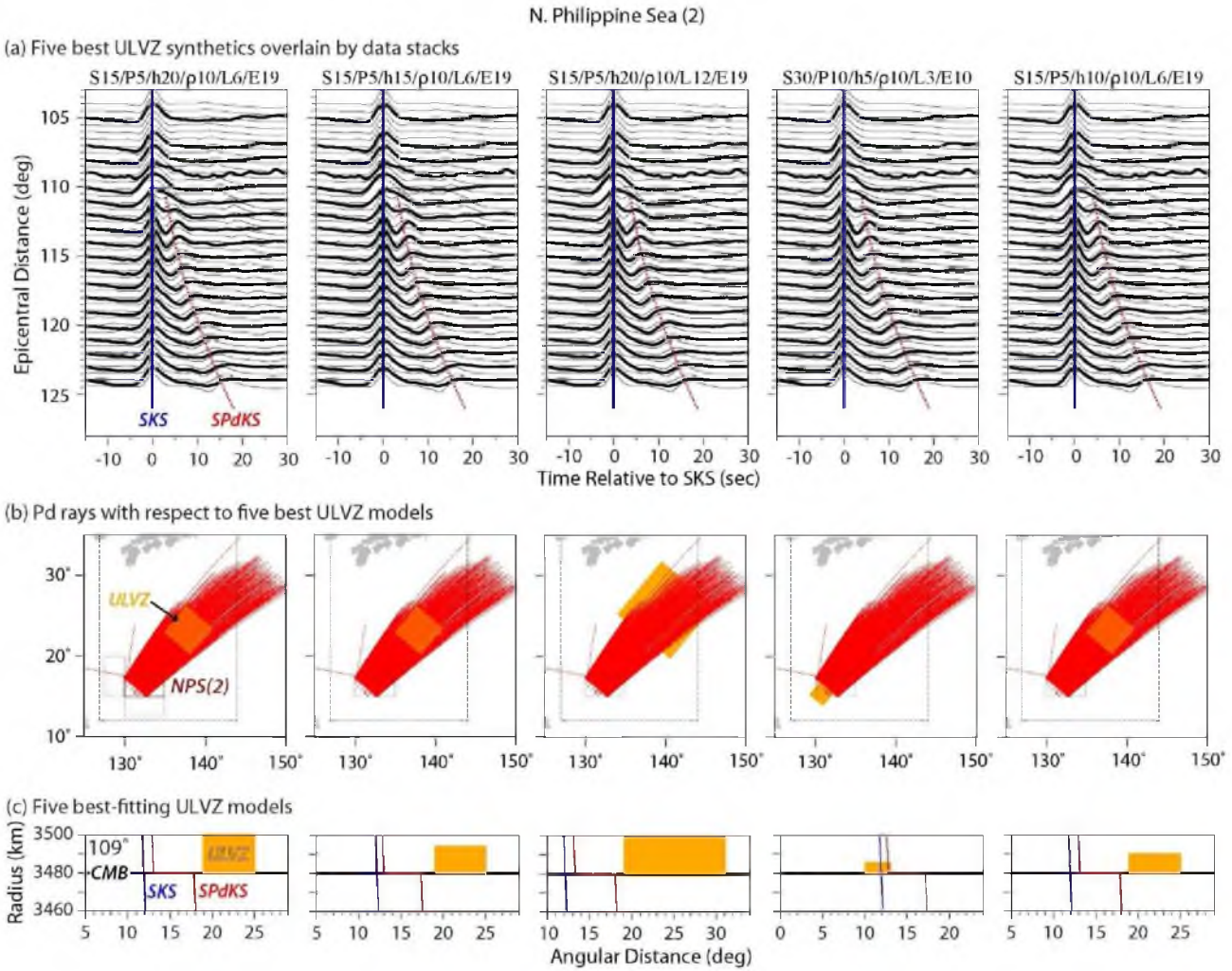

Figure A.17. N. Philippine Sea Region 2

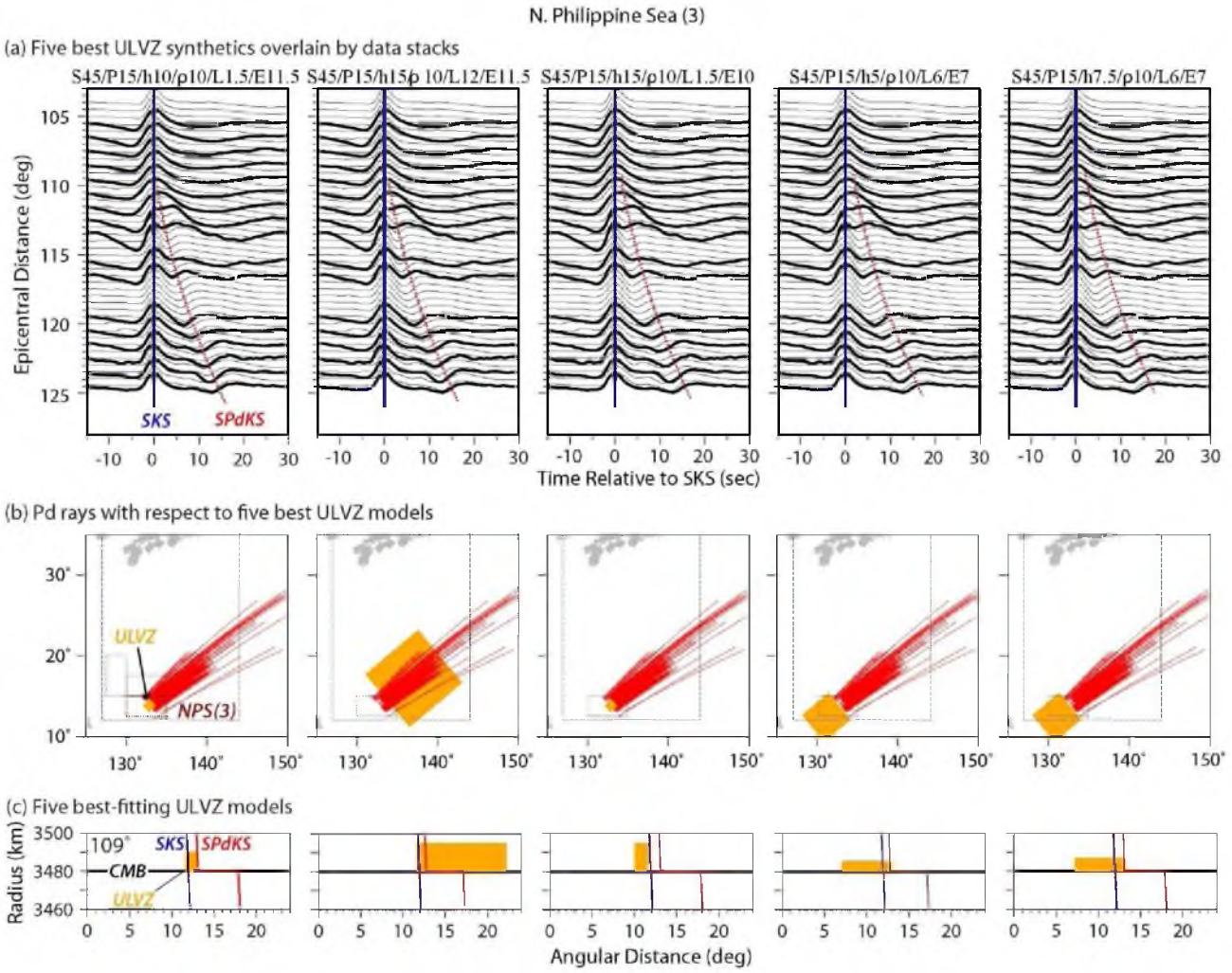

Figure A.18. N. Philippine Sea Region 3

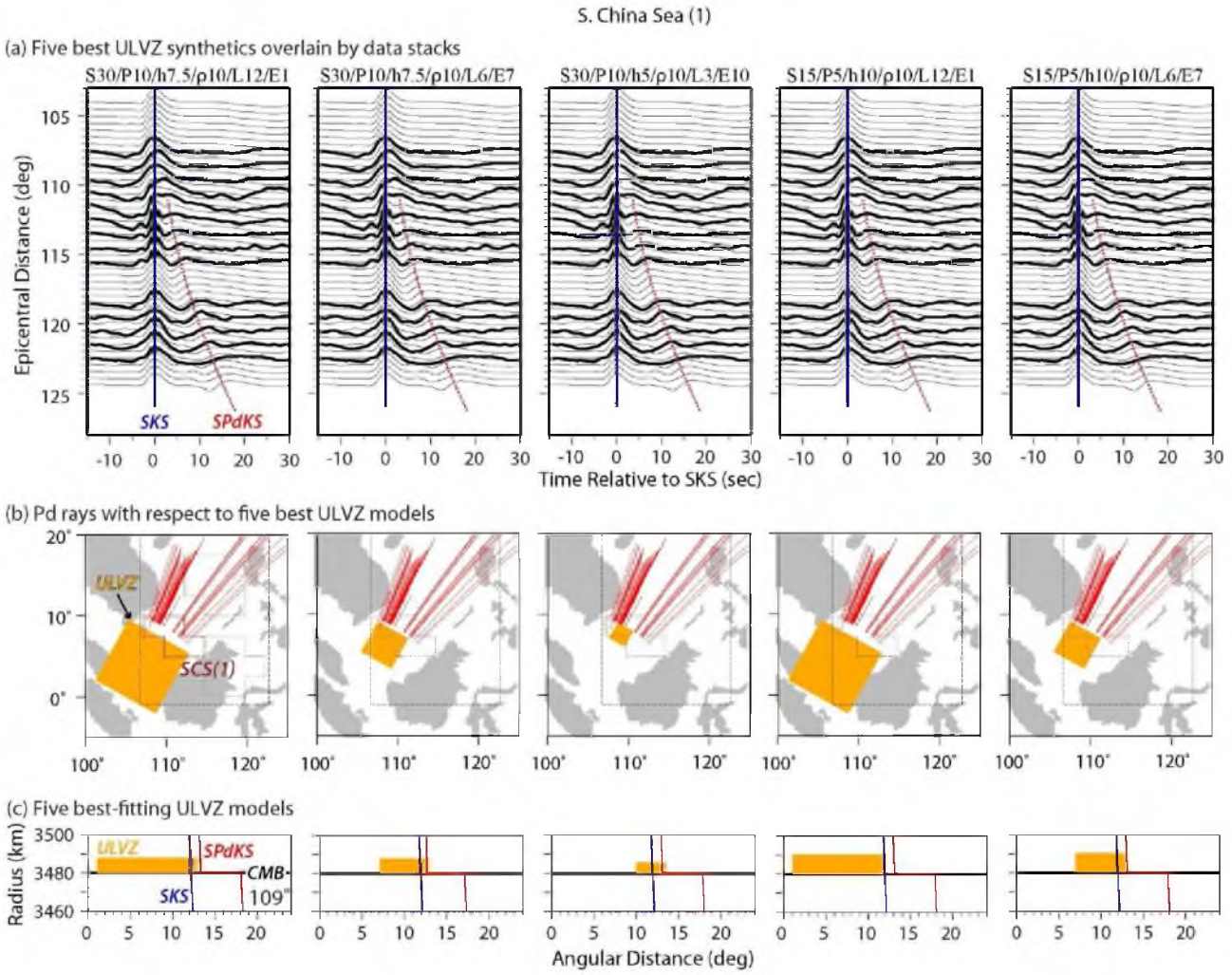

Figure A.19. S. China Sea Region 1

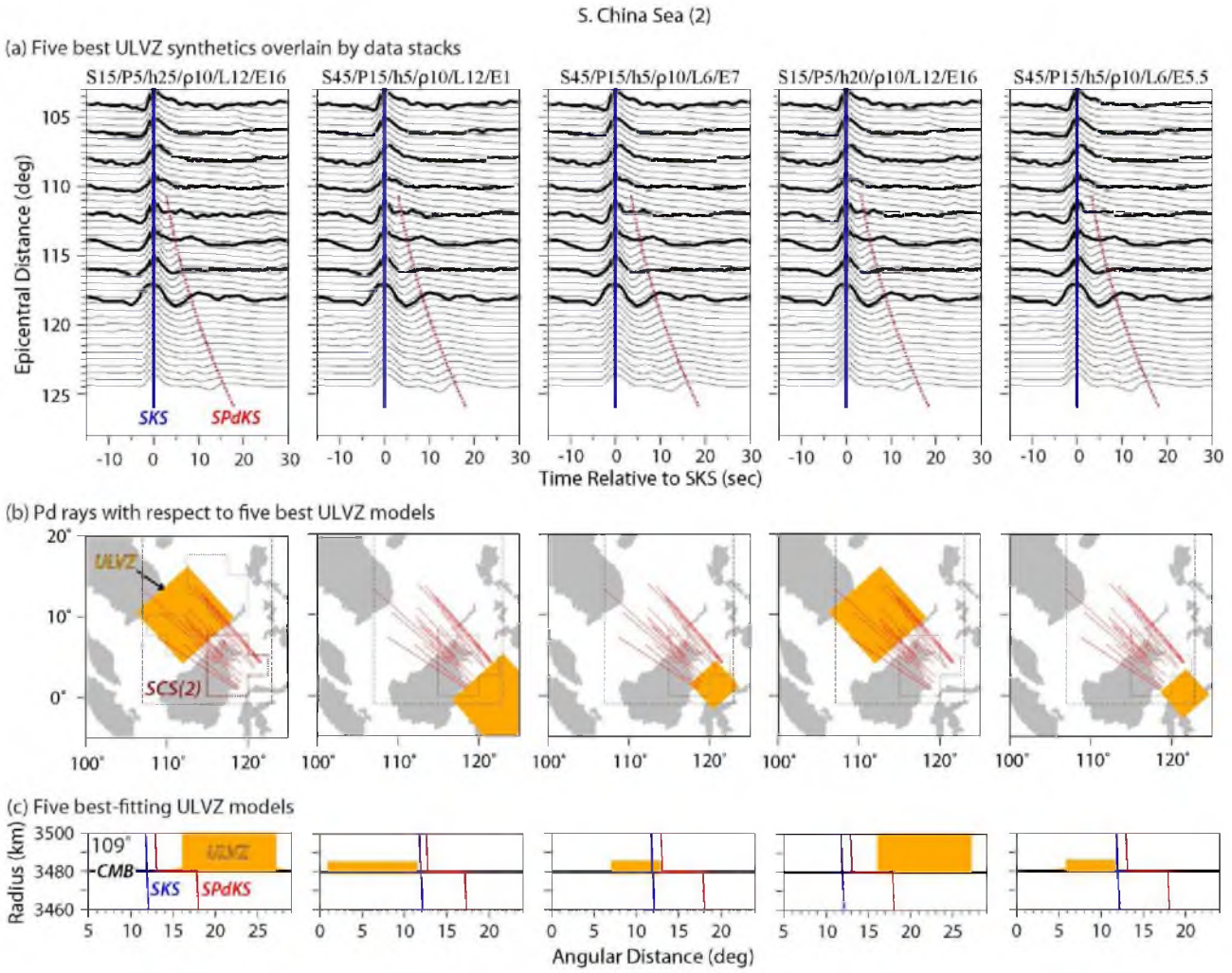

Figure A.20. S. China Sea Region 2

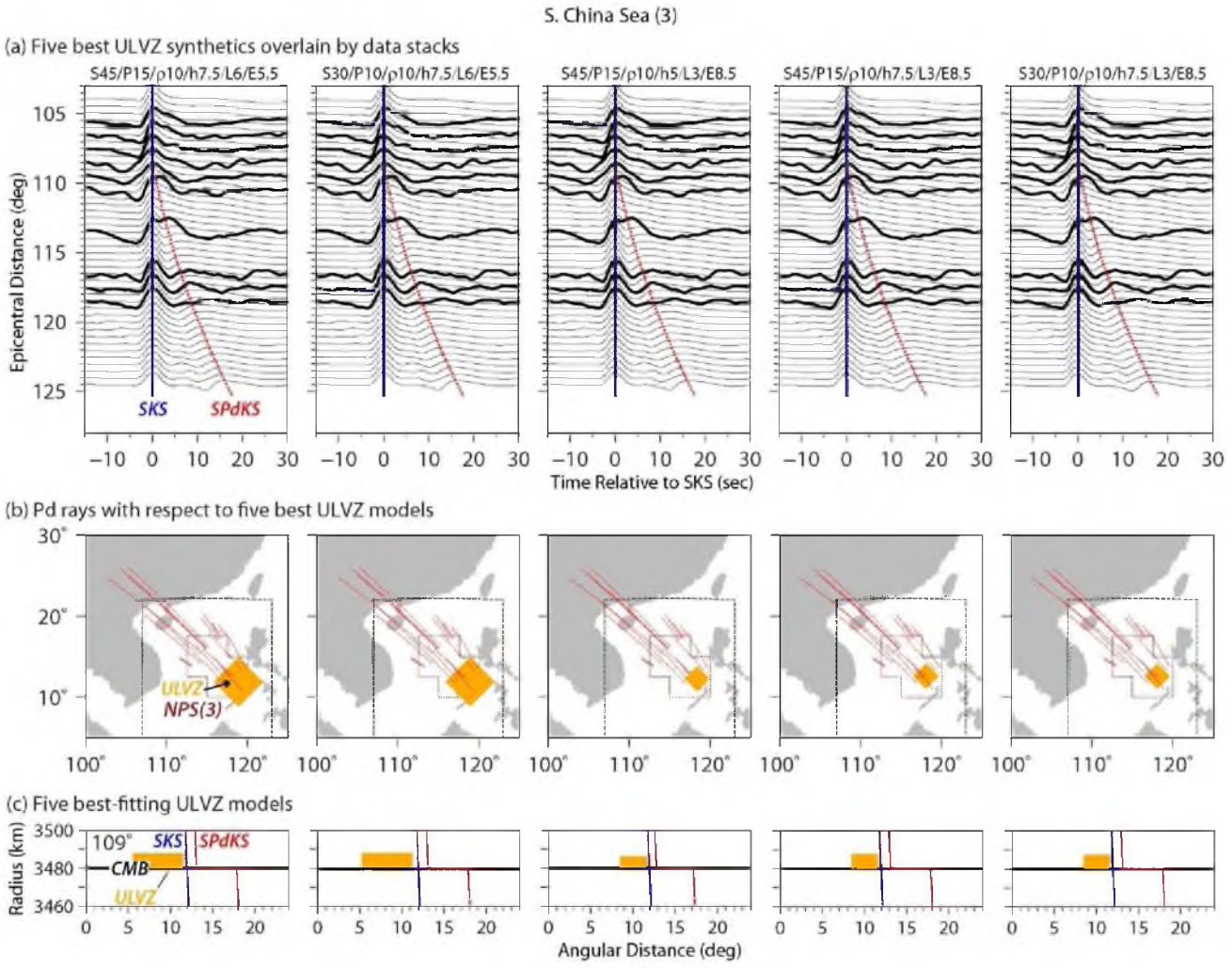

Figure A.21. S. China Sea Region 3

Figures A.22 – A.23 show additional ULVZ models that fit the data for the SCS1 region from 104° - 125° within 90% confidence of the best-fit m odel. Aligned on *SKS*, the data stacks are black traces, UVLZ model synthetics are gray traces, with *SKS* and *SKPdS* arrivals marked by dotted black and gray lines respectively. The parameters used here, and the labeling style is the same as for the waveform comparisons in Figures A.14 – A.21. Scrutiny of the waveforms reveals close similarities in the synthetic signals. Each of these models predict that the Pd paths of *SPdKS* in these areas interact with an ULVZ in similar geospatial ways; they interact with predicted ULVZ that are of similar thickness, and with approximately the same lateral extent of the ULVZ.

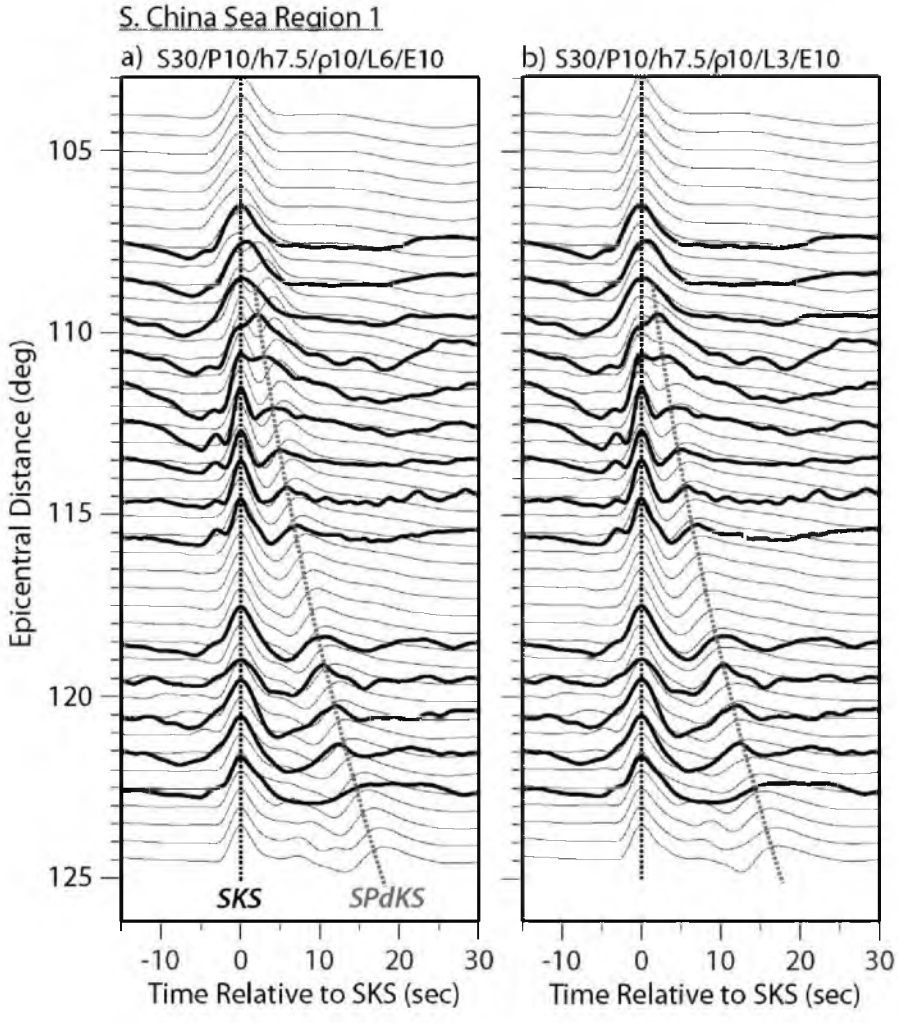

Figure A.22. S. China Sea Region 1

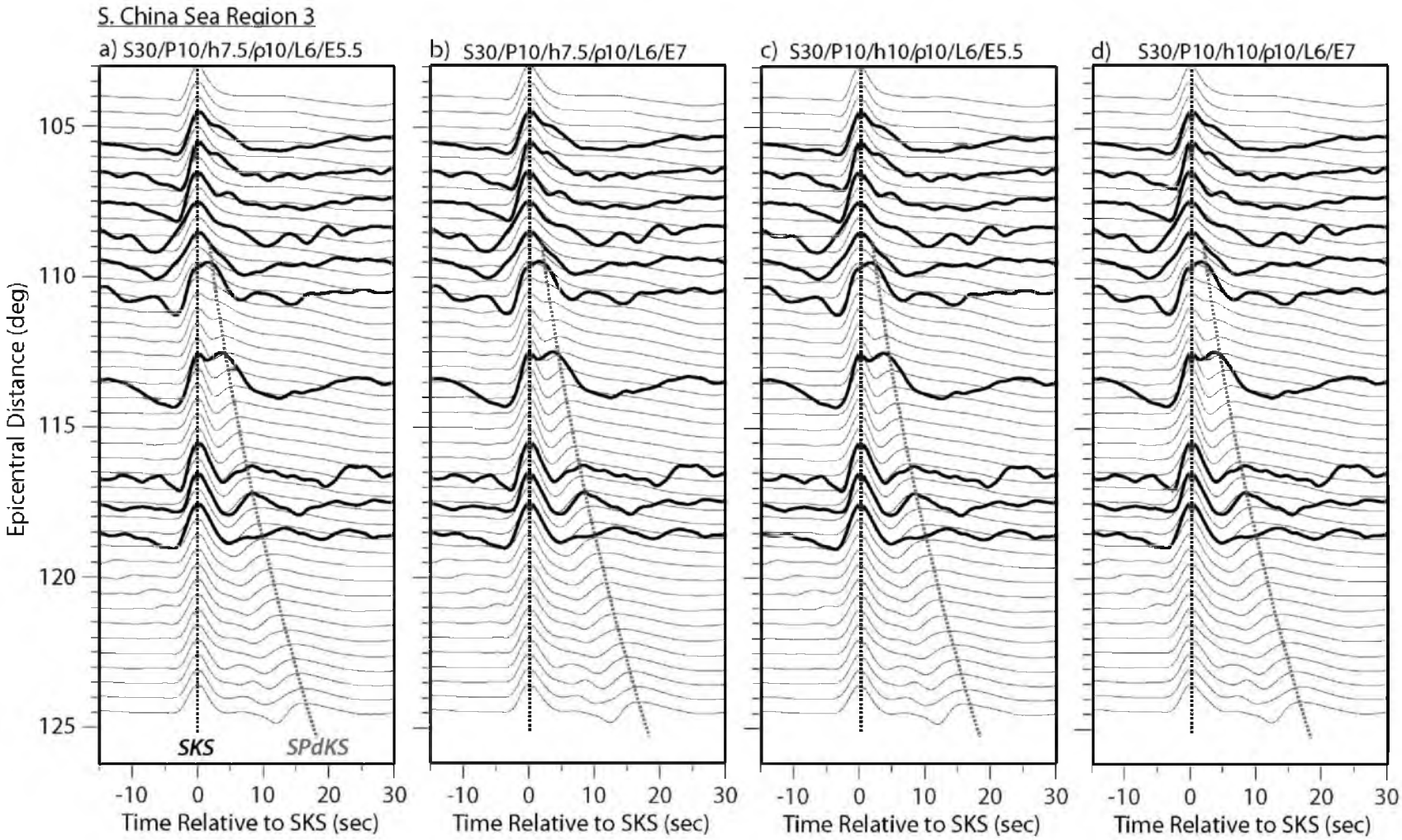

Figure A.23. S. China Sea Region 3

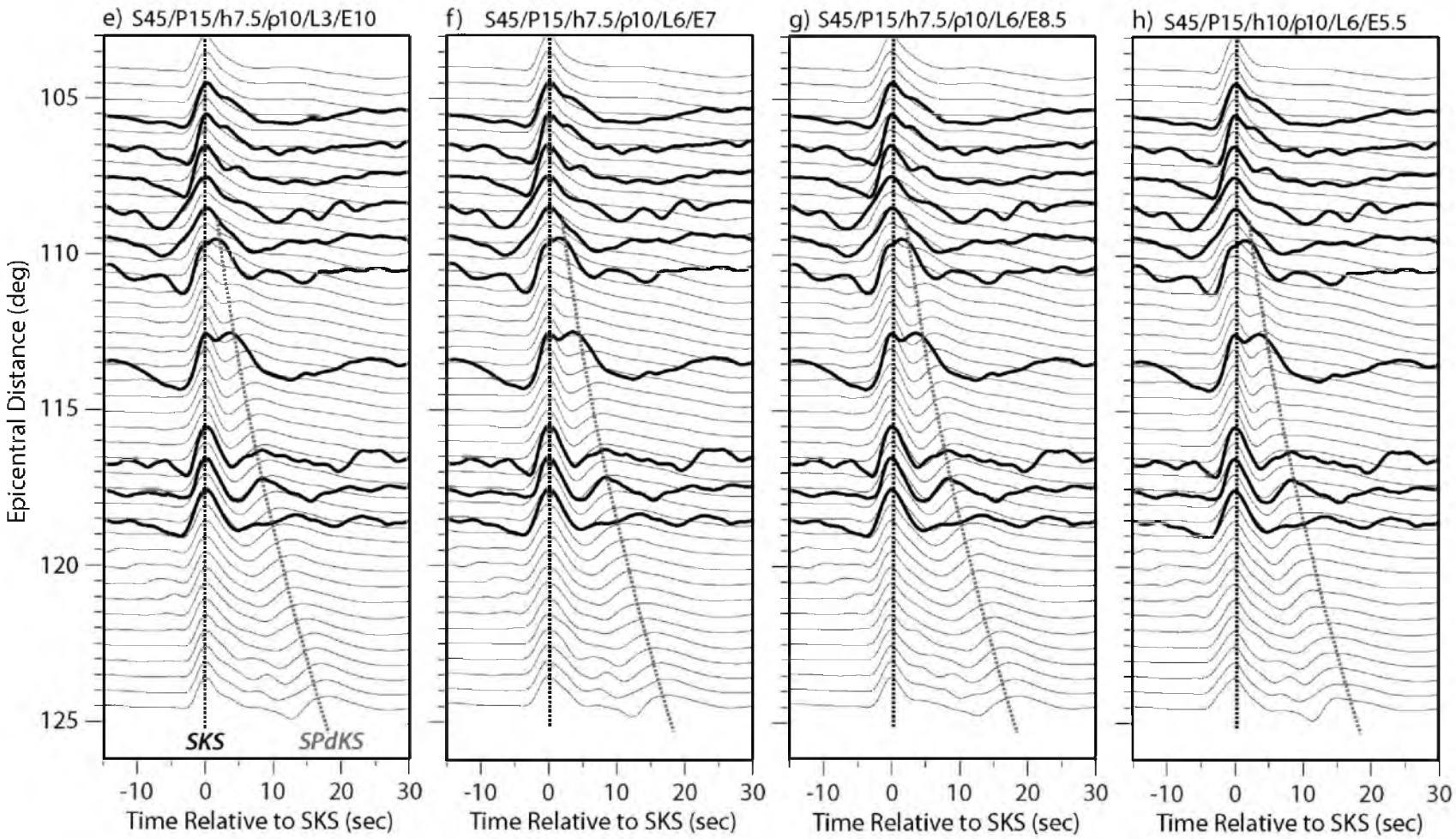

Figure A.23. Continued.

Table A1. Earthquakes used in this study.

Event	Date	Latitude, deg	Longitude, deg	Depth, km	Mw
1	18 MAY, 1993	19.8	122.5	214	6.1
2	7 AUG, 1993	-23.9	179.8	555	6
3	25 DEC, 1995	-6.9	129.2	150	6.2
4	28 FEB, 1996	1.7	126.1	103	6.1
5	5 NOV, 1996	-31.2	180	369	5.9
6	1 DEC, 1996	-30.5	-179.7	356	6.1
7	21 MAR, 1997	-31.2	179.6	449	6.3
8	23 APR, 1997	14	144.9	101	6.2
9	3 MAY, 1997	-31.8	-179.4	108	6.6
10	4 SEP, 1997	-26.6	178.3	625	6.3
11	23 MAY, 1998	8.1	123.7	658	5.9
12	9 JUL, 1998	-30.5	-179	130	6.2
13	27 DEC, 1998	-21.6	-176.4	144	6.1
14	9 APR, 1999	-26.4	178.2	621	6.2
15	3 MAR, 2000	-7.3	128.5	142	6.4
16	10 JUL, 2000	-4.5	103.8	105	5.8
17	15 JUL, 2000	-7	128.9	218	5.9
18	16 FEB, 2001	-7.2	117.5	521	5.9
19	19 MAR, 2002	-6.5	129.9	148	6.1
20	5 MAY, 2003	0.2	127.4	124	5.9
21	25 JUL, 2004	-2.4	104	582	6.8
22	5 FEB, 2005	5.3	123.3	525	6.4
23	15 OCT, 2005	25.3	123.4	183	6.2
24	15 JAN, 2006	-7.8	122.6	265	6
25	26 FEB, 2006	-23.6	-180	535	5.9
26	15 JUL, 2006	-4.5	126.2	368	5.8
27	14 NOV, 2006	-6.4	128	352	6.1
28	23 JUL, 2007	-4.5	149.9	572	5.9
29	25 SEP, 2007	-31	180	417	6.2
30	29 APR, 2008	-6.1	127.5	405	5.9
31	26 APR, 2009	-30.3	-178.6	132	6.1
32	4 OCT, 2009	6.7	123.4	620	6.4
33	24 OCT, 2009	-6.1	130.4	130	6.7
34	22 NOV, 2009	-31.6	179.5	436	6.2
35	16 MAY, 2010	0.5	124.7	123	5.8
36	17 JUN, 2010	-33.2	179.7	170	6.0
37	21 JUL, 2010	3.0	128.2	100	6.0
38	23 JUL, 2010	6.5	123.5	586	6.9
39	24 JUL, 2010	6.2	123.5	553	5.9
40	29 JUL, 2010	6.5	123.2	627	6.1

Table A.2. Data analysis of *SPdKS* bins.

Bin	# of Models in 95% CI*	# of Models in 90% CI*	# of Models in 80% CI*	# of Models in 70% CI*	# of Data Stacks	# of Data Traces
Coral Sea	3	4	7	14	11	56
S. Philippine Sea	2	3	***7***	20	21	358
N. Philippine Sea (1)	10	24	57	104	12	46
N. Philippine Sea (2)	1	2	2	13	19	565
N. Philippine Sea (3)	3	14	48	105	17	230
S. China Sea (1)	4	11	34	***61***	14	54
S. China Sea (2)	10	18	43	***91***	8	25
S. China Sea (3)	1	1	1	1	10	20

*Confidence Interval. Bold italic numbers represent the CI in which the PREM model lies. Each of the CIs are cumulative (i.e., that one model in the 95% and 90% CIs for the Coral Sea bin is the same model, while the 80% CI contains the previous one and adds two).

REFERENCES

Avants, M., T. Lay, and E. J. Garnero (2006), A new probe of ULVZ S-wave velocity structure: Array stacking of ScS waveforms, *Geophys. Res. Lett.*, *33*(L07314), doi: 10.1029/2005GL024989.

Berryman, J. G. (2000), Seismic velocity decrement ratios for regions of partial melt in the lower mantle, *Geophys. Res. Lett.*, *27*(3), 421-424, doi: 10.1029/1999GL008402.

Dziewonski, A. M., and D. L. Anderson (1981), Preliminary reference Earth model, *Phys. Earth Planet. Inter.*, *25*, 297-356.

Garnero, E. J., and D. V. Helmberger (1995), A very slow basal layer underlying large-scale low-velocity anomalies in the lower mantle beneath the Pacific: evidence from core phases, *Phys. Earth Planet. Inter.*, *91*, 161-176.

Garnero, E. J., and D. V. Helmberger (1996), Seismic detection of a thin laterally varying boundary layer at the base of the mantle beneath the central-Pacific, *Geophys. Res. Lett.*, *23*(9), 977-980.

Garnero, E. J., and D. V. Helmberger (1998), Further structural constraints and uncertainties of a thin laterally varying ultralow-velocity layer at the base of the mantle, *J. Geophys. Res.*, *103*(B6), 12495-12509.

Garnero, E. J., and J. E. Vidale (1999), *ScP*; a probe of ultralow velocity zones at the base of the mantle, *Geophys. Res. Lett.*, *26*(3), 377-380.

Garnero, E. J., and A. K. McNamara (2008), Structure and dynamics of earth's lower mantle, *Science*, *320*, 626-628, doi: 10.1126/science.1148028.

Garnero, E. J., S. P. Grand, and D. V. Helmberger (1993), Low P-wave velocity at the base of the mantle, *Geophys. Res. Lett.*, *20*(17), 1843-1846.

Hutko, A. R., T. Lay, and J. Revenaugh (2009), Localized double-array stacking analysis of PcP: D" and ULVZ structure beneath the Cocos plate, Mexico, central Pacific, and north Pacific, *Phys. Earth Planet. Inter.*, *173*, 60-74, doi: 10.1016/j.pepi.2008.11.003.

Idehara, K. (2011), Structural heterogeneity of an ultra-low-velocity zone beneath the Philippine Islands: Implications for core–mantle chemical interactions induced by massive partial melting at the bottom of the mantle, *Phys. Earth Planet. Inter.*, *184*, 80-90, doi: 10.1016/j.pepi.2010.10.014.

Idehara, K., A. Yamada, and D. Zhao (2007), Seismological constraints on the ultralow velocity zones in the lowermost mantle from core-reflected waves, *Phys. Earth Planet. Inter.*, *165*, 25-46, doi: 10.1016/j.pepi.2007.07.005.

Mao, W. L., H.-k. Mao, W. Sturhahn, J. Zhao, V. B. Prakapenka, Y. Meng, J. Shu, Y. Fei, and R. J. Hemley (2006), Iron-rich post-perovskite and the origin of ultralow-velocity zones, *Science*, *312*, 564-565.

McNamara, A. K., E. J. Garnero, and S. Rost (2010), Tracking deep mantle reservoirs with ultra-low velocity zones, *Earth Planet. Sci. Lett.*, *299*, 1-9, doi: 10.1016/j.epsl.2010.07.042.

Mori, J., and D. V. Helmberger (1995), Localized boundary layer below the mid-Pacific velocity anomaly identified from a PcP precursor, *J. Geophys. Res.*, *100*(B10), 20359-20365.

Reasoner, C., and J. Revenaugh (2000), *ScP* constraints on ultralow-velocity zone density and gradient thickness beneath the Pacific, *J. Geophys. Res.*, *105*(B12), 28173-28182.

Revenaugh, J., and R. Meyer (1997), Seismic evidence of partial melt within a possibly ubiquitous low-velocity layer at the base of the mantle, *Science*, *277*, 670-673.

Rondenay, S., V. F. Cormier, and E. M. Van Ark (2010), *SKS* and *SPdKS* sensitivity to two-dimensional ultralow-velocity zones, *J. Geophys. Res.*, *115*(B04311), doi: 10.1029/2009JB006733.

Rost, S., and J. Revenaugh (2001), Seismic detection of rigid zones at the top of the core, *Science*, *294*, 1911-1914.

Rost, S., and J. Revenaugh (2003), Small-scale ultralow-velocity zone structure imaged by *ScP*, *J. Geophys. Res.*, *108*(B1), doi: 10.1029/2001JB001627.

Rost, S., E. J. Garnero, and Q. Williams (2006), Fine-scale ultralow-velocity zone structure from high-frequency seismic array data, *J. Geophys. Res.*, *111*(B09310), doi: 10.1029/2005JB004088.

Rost, S., E. J. Garnero, and W. Stefan (2010), Thin and intermittent ultralow-velocity zones, *J. Geophys. Res.*, *115*(B06312), doi: 10.1029/2009JB006981.

Rost, S., E. J. Garnero, Q. Williams, and M. Manga (2005), Seismological constraints on a possible plume root at the core-mantle boundary, *Nature*, *435*, 666-669, doi: 10.1038/nature03620.

Thomas, C., M. Weber, C. W. Wicks, and F. Scherbaum (1999), Small scatterers in the lower mantle observed at German broadband arrays, *J. Geophys. Res.*, *104*(B7), 15073-15088.

Thorne, M. S., and E. J. Garnero (2004), Inferences on ultralow-velocity zone structure from a global analysis of *SPdKS* waves, *J. Geophys. Res.*, *109*, doi: 10.1029/2004JB003010.

Thorne, M. S., Y. Zhang, and J. Ritsema (2013a), Evaluation of 1D and 3D seismic models of the Pacific lower mantle with S, *SKS*, and *SKKS* traveltimes and amplitudes, *J. Geophys. Res.*, *118*, 1-11, doi: 10.1002/jgrb.50054.

Thorne, M. S., E. J. Garnero, G. Jahnke, H. Igel, and A. K. McNamara (2013b), Mega ultra low velocity zone and mantle flow, *Earth Planet. Sci. Lett.*, *364*, 59-67, doi: 10.1016/j.epsl.2012.12.034.

Vidale, J. E., and M. A. H. Hedlin (1998), Evidence for partial melt at the core-mantle boundary north of Tonga from the strong scattering of seismic waves, *Nature*, *391*, 682-685.

Wen, L. (2001), Seismic evidence for a rapidly varying compositional anomaly at the base of the Earth's mantle beneath the Indian Ocean, *Earth Planet. Sci. Lett.*, *194*, 83-95.

Wen, L., and D. V. Helmberger (1998), A two-dimensional P-SV hybrid method and its application to modeling localized structures near the core-mantle boundary, *J. Geophys. Res.*, *103*(B8), 17901-17918.

Wessel, P., and W. H. F. Smith (1998), New, improved version of Generic Mapping Tools released, *EOS transactions*, *79*, 579-579.

Wicks, J. K., J. M. Jackson, and W. Sturhahn (2010), Very low sound velocities in iron-rich (Mg,Fe)O: Implications for the core-mantle boundary region, *Geophys. Res. Lett.*, *37*(L15304), doi: 10.1029/2010GL043689.

Williams, Q., and E. J. Garnero (1996), Seismic evidence for partial melt at the base of Earth's mantle, *Science*, *273*, 1528-1530.

Xu, Y., and K. D. Koper (2009), Detection of a ULVZ at the base of the mantle beneath the northwest Pacific, *Geophys. Res. Lett.*, *36*(L17301), doi: 10.1029/2009GL039387.

Zhang, Y., J. Ritsema, and M. S. Thorne (2009), Modeling the ratios of *SKKS* and *SKS* amplitudes with ultra-low velocity zones at the core-mantle boundary, *Geophys. Res. Lett.*, *36*(L19303), doi: 10.1029/2009GL040030.